

Pulsed optically pumped ^{87}Rb vapor cell frequency standard: A multilevel approach

Salvatore Micalizio, Aldo Godone, Filippo Levi, and Claudio Calosso
Istituto Nazionale di Ricerca Metrologica, INRIM, Strada delle Cacce 91, 10135 Torino, Italy

(Received 23 October 2008; published 6 January 2009)

We present a multilevel theoretical approach to describe the behavior of a pulsed optically pumped (POP) ^{87}Rb frequency standard based on a microwave cavity-vapor cell arrangement. The full Zeeman manifold of the ground-state hyperfine levels is then considered, and the dynamics induced among them by relaxation processes (buffer gas, spin exchange, and cell-walls collisions) is taken into account. The model includes as well the absorption of the pumping laser along the cell and the cavity feedback on the atoms; the effects related to a nonuniform excitation of the atomic sample are also discussed. Theoretical predictions are proven with a laboratory prototype of POP passive maser in which the clock transition is excited by means of the Ramsey technique. The agreement between theory and experiment is very satisfactory from both a quantitative and qualitative point of view, in terms of the shape of the Ramsey fringes, microwave power delivered by the atoms, and short-term frequency stability. In particular, a frequency stability of 1.2×10^{-12} at one second has been measured, in very good agreement with the expected value. On this basis, the model has been extended to predict the short-term frequency stability of a POP frequency standard operating with optical detection. A shot-noise limited frequency stability (Allan deviation) of $\sigma_y(\tau) \approx 3 \times 10^{-14} \tau^{-1/2}$ is foreseen. This value can be degraded by microwave phase noise and laser fluctuations so that the overall predicted clock stability is $\sigma_y(\tau) \approx 1.5 \times 10^{-13} \tau^{-1/2}$.

DOI: [10.1103/PhysRevA.79.013403](https://doi.org/10.1103/PhysRevA.79.013403)

PACS number(s): 32.80.Xx, 06.30.Ft, 32.30.Bv

I. INTRODUCTION

Pulsing the different operation phases of a laser pumped vapor cell frequency standard has been recently recognized as one of the most effective techniques to reduce light shift and then to improve the stability perspectives of these clocks [1]. In particular, the pulsed optically pumped (POP) rubidium maser has achieved very interesting results in this regard. In fact, a frequency stability (Allan deviation) of $\sigma_y(\tau) = 1.2 \times 10^{-12} \tau^{-1/2}$ for integration times up to $\tau = 10^5$ s has been measured, and the 10^{-15} region, after drift removal, has been reached [2]. This result is among the best achieved by a vapor cell frequency standard, and it is comparable to the stability performance of a H passive maser.

The POP clock concept relies on the time separation of the phases of optical pumping, interrogation, and detection of the clock transition, so that the atoms experience the laser light during the pumping phase only; transfer of the laser noise to the clock transition is strongly reduced with respect to the continuous operation case, and in this way light shift is made negligible. The schematic setup that implements these three operation phases is shown in Fig. 1(a) and the timing sequence is shown in Fig. 1(b).

The original idea of pulsed optical pumping dates back to the 1960s [3], and we recently reconsidered it since the current technological devices, mainly diode lasers and dedicated digital electronics, allow a very effective implementation of this powerful idea.

The theory developed in our previous works [2,4] is based mainly on the following assumptions:

(i) A sample of ^{87}Rb atoms is contained in a cell with buffer gas and placed in a high- Q resonant microwave cavity. ^{87}Rb is modeled as a three-level atom: two ground-state hyperfine levels defining the clock transition and an excited state in resonance with the laser field.

(ii) The atom-field interaction includes the laser field for the optical pumping and the microwave field for the interrogation of the clock transition; in particular, the interrogation is performed with two separated microwave pulses defining the Ramsey excitation scheme.

(iii) The clock transition is detected at the end of the second Ramsey pulse through the free induction decay [5] signal, which is proportional to the hyperfine coherence excited between the two ground-state levels.

(iv) The relaxation phenomena due to the buffer gas collisions, spin exchange collisions, and cell-walls collisions after diffusion through the buffer gas have been taken into account in a phenomenological way introducing proper relaxation rates for the hyperfine coherence and for the atomic populations, without considering the actual dynamics of the relaxation processes.

(v) The atomic medium has been assumed thin.

The main physical features of the POP maser are well described from a qualitative point of view in terms of this model: it predicts among other things that the light shift can be made negligible and that cavity pulling can be strongly attenuated with a proper choice of the microwave pulse amplitude [2]. However, this model fails when a quantitative comparison between theory and experiment is made. In fact, the three-level approximation leads to an overestimate of the output power delivered by the atoms with respect to that experimentally measured. Moreover, the observed complete Ramsey pattern shows some peculiar shapes that are not fully described by the Ramsey fringes calculated with the three-level model.

In this work, we study a multilevel approach to include the full Zeeman manifold of the ground-state hyperfine levels. In this context, the relaxation phenomena are not simply introduced in a phenomenological way, but we take into account that Rb buffer gas collisions, Rb-Rb collisions (spin

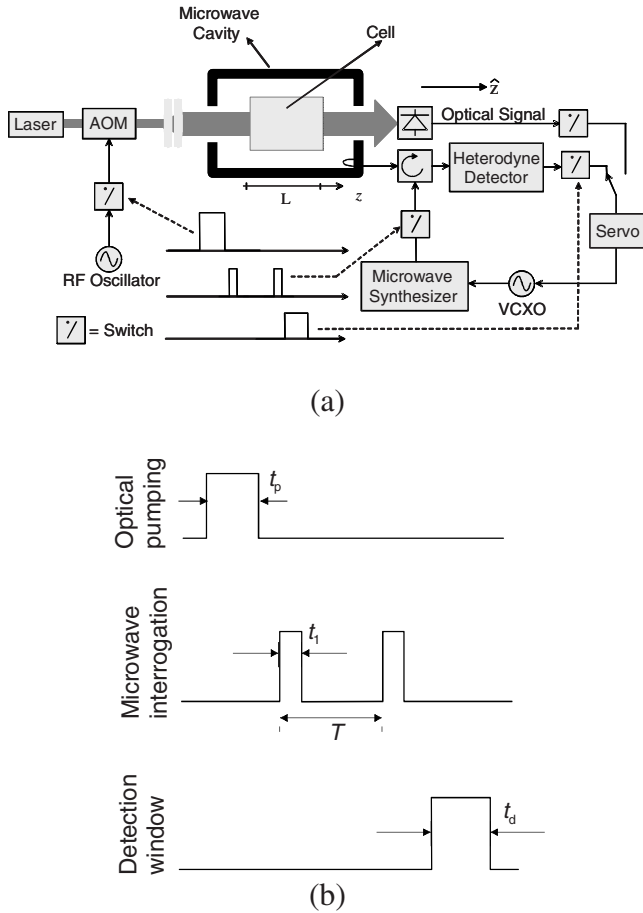


FIG. 1. (a) Schematic setup of the POP frequency standard. AOM: acousto-optic modulator. VCXO: voltage controlled crystal oscillator; (b) timing sequence, where t_p , t_1 , T , and t_d are, respectively, the pumping, Rabi pulses, Ramsey decay, and detection times.

exchange), and the diffusion motion of the atoms through the buffer gas induce a precise dynamics in the atomic populations distribution; this dynamics plays an important role in determining the behavior of the system. Moreover, we will extend our analysis also to the case of a thick atomic medium (the absorption of the laser while propagating into the cell is then considered).

This more accurate model is able to predict very well the experimental observations, not only concerning the power level and the Ramsey pattern, but also the transient regimes: the time evolution of the physical quantities (populations and coherences) during the different operation phases is much better fitted.

Moreover, the multilevel approach also explains a residual frequency shift related to the change of the light intensity. This effect, the so called “position-shift” [6], is related to the inhomogeneity of the physics package and/or to a non-spatially-symmetric excitation of the atomic sample, and here we provide a clear description and measure of it.

In this paper, we discuss as well the possibility to detect the clock transition in the optical domain in the framework of this multilevel system. The detection of a transmitted optical probe may lead in fact to some advantages with respect

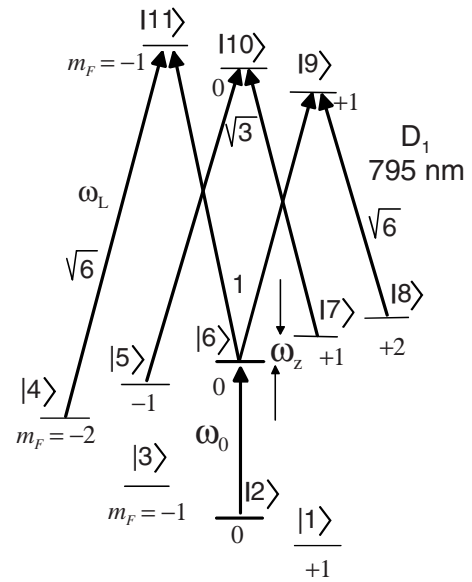


FIG. 2. Atomic levels of ^{87}Rb involved in the optical pumping; ω_L and ω_0 are the angular laser and microwave frequencies; ω_z is the (angular) frequency between neighboring Zeeman levels. The optical relative transition strengths are also indicated.

to the microwave detection, due to the higher energy of the optical photons with respect to the microwave ones. It is possible in fact to operate the clock at a lower temperature (that implies a lower atomic density) with a higher signal-to-noise ratio and with reduced cavity-pulling, spin exchange, and position shift effects.

Following the guidelines of the multilevel model here reported, it is possible in principle to develop a frequency standard with stability performances similar to that of an active H-maser, but with an easier and more reliable technical implementation, of particular interest for on-board space applications.

II. THEORY

We consider a linearly polarized laser tuned to the ^{87}Rb $|^2S_{1/2}; F=2\rangle - |^2P_{1/2}; F'=1\rangle$ component of the D_1 optical transition. For simplicity, we assume that the laser detuning is zero. This assumption does not allow us to evaluate the FM-FM and the FM-AM static conversion factors describing the changes of the frequency and of the amplitude of the clock signal due to a change of the laser frequency. As far as the FM-FM conversion is concerned (resonant light-shift), it is known to be marginal in the pulsed operation [2]; as regards the FM-AM conversion, it may play a role only in the case of optical detection and will be considered further on.

We also assume that the optical pumping does not involve the other component of the D_1 line with $F'=2$ that is separated by more than one homogeneous linewidth. The wave vector is parallel to the quantization axis defined by a static magnetic field $\mathbf{B}_0 = B_0 \hat{z}$. The two circular components σ^+ and σ^- of the linearly polarized laser couple the $\Delta m_F = 1$ and -1 sublevel transitions, respectively, according to the scheme of Fig. 2.

The atomic medium is a low-pressure Rb vapor contained in a cylindrical quartz cell with buffer gas that is placed in a microwave cavity operating in the TE_{011} mode and tuned to the ground-state hyperfine frequency. After the optical pumping phase, a standing-wave microwave field is applied to the system at a frequency corresponding to the transition levels $|2\rangle = |F=1; m_F=0\rangle$ and $|6\rangle = |F=2; m_F=0\rangle$; we assume that no other hyperfine coherence is excited in the atomic sample.

The coupling of the atoms to the radiation fields is described in terms of Maxwell-Bloch equations that, in compact form, we can write as

$$\frac{\partial \hat{\rho}}{\partial t} = D\nabla^2 \hat{\rho} - \frac{i}{\hbar} [\hat{H}, \hat{\rho}], \quad (1)$$

$$\nabla \times \nabla \times \mathbf{H}^{\mu w} + \frac{1}{c^2} \frac{\partial^2 \mathbf{H}^{\mu w}}{\partial t^2} = -\frac{1}{c^2} \frac{\partial^2 \mathbf{M}}{\partial t^2}, \quad (2)$$

$$\nabla \times \nabla \times \mathbf{E} + \frac{1}{c^2} \frac{\partial^2 \mathbf{E}}{\partial t^2} = -\mu_0 \frac{\partial^2 \mathbf{P}}{\partial t^2}. \quad (3)$$

The first equation is a Liouville-type equation and describes the time evolution of the atomic density matrix $\hat{\rho}$ under the action of the Hamiltonian \hat{H} .

The Hamiltonian \hat{H} is the sum of several contributions,

$$\hat{H} = \hat{H}_0 + \hat{H}_E + \hat{H}_{\mu w} + \hat{H}_{\text{bg}} + \hat{H}_{\text{se}}, \quad (4)$$

where (i) \hat{H}_0 is the unperturbed Hamiltonian containing also the static perturbations such as Zeeman effect and Stark shift, (ii) \hat{H}_E considers the interaction with the laser field, (iii) $\hat{H}_{\mu w}$ describes the interaction with the microwave field, (iv) \hat{H}_{bg} describes the interaction taking place during a collision between the excited atom and the buffer gas atom or molecule, and (v) \hat{H}_{se} takes into account the interaction that a couple of Rb atoms experience while colliding with each other (spin-exchange collision).

Concerning Eq. (1), complete relaxation of the atoms is assumed when they reach the uncoated wall of the cell by diffusion through the buffer gas: D is the diffusion coefficient, inversely dependent on the buffer gas pressure P and defined as

$$D = D_0 \frac{P_0}{P}, \quad (5)$$

where D_0 is the diffusion constant of Rb atoms in the considered buffer gas and P_0 is equal to 760 Torr.

We observe that in a three-level approximation, the system reduces to the two hyperfine clock levels, $|2\rangle$ and $|6\rangle$ in Fig. 2, and one excited state. The relaxation is basically described by two phenomenological relaxation rates, one for the population difference of the clock levels (we call it γ_1) and one for the coherence excited between them (γ_2) [7]. Under the action of relaxation, population difference and coherence tend to their equilibrium value that is zero for both; γ_1 and γ_2 can be easily written summing up the coefficients due to each relaxation source, and no memory of the origin of each relaxation contribution is necessary to describe the

physical behavior. In the multilevel approach, it is instead important to distinguish among the different relaxation processes since buffer gas and spin exchange induce a precise dynamics among the ground-state sublevels. As a consequence of buffer gas collisions, we will see, for example, that only certain transitions take place inside the Zeeman manifold of the ground state [5]. Moreover, it may be important to know if buffer gas collisions are only of binary type or if the process of molecule formation is relevant in a given physical condition. Similar considerations also hold for the spin exchange that is responsible as well for a nontrivial redistribution of the ground-state atomic populations toward their equilibrium value ($\rho_{\mu\mu} \rightarrow 1/8$, $\mu=1-8$).

For this reason, buffer gas and spin-exchange collisions are more properly described with the respective Hamiltonians.

Equations (2) and (3) are the Maxwell equations taking into account that a magnetization \mathbf{M} and a polarization \mathbf{P} are excited in the atomic medium. In particular, Eq. (2) with proper boundary conditions leads to the Slater equation [5] for the magnetic field $\mathbf{H}^{\mu w}$ sustained in the cavity, while Eq. (3) describes the dynamics of the laser electric field \mathbf{E} during the pumping process and should be considered also when the optical transmission signal is used to detect the clock transition.

The source terms in Eqs. (2) and (3) are obviously expressed in terms of the density-matrix elements as expectation values of the magnetization and polarization operators. Equations (1)–(3) are then a system of coupled equations that completely describe the dynamics in which we are interested; μ_0 is the vacuum permeability, c is the speed of light in vacuum, and \hbar is the reduced Planck constant.

In the following, we report in detail all the physical considerations necessary to write the system (1)–(3) in an explicit form suitable for the numerical evaluation of the most significant physical quantities required to describe the POP frequency standard.

A. Interaction atom-laser field: \hat{H}_E

The laser light is described by a classical field of (angular) frequency ω_L , with definite polarization $\hat{\mathbf{e}}$ and propagating along the z axis, so that $\mathbf{k}_L \cdot \hat{\mathbf{z}} = k_L$, \mathbf{k}_L being the wave vector,

$$\mathbf{E}(t) = \frac{E_0(z, t)}{2} \hat{\mathbf{e}} e^{i(\omega_L t - k_L z + \phi(z, t))} + \text{c.c.} \quad (6)$$

In Eq. (6), $\phi(z, t)$ is a general phase term accounting for the laser linewidth [8] and $E_0(z, t)$ is the field amplitude, both slowly dependent on z and t and without radial dependence.

The interaction Hamiltonian is written in the usual form $\hat{H}_E = \hat{\mathbf{d}} \cdot \mathbf{E}(t)$, where $\hat{\mathbf{d}} = -e\hat{\mathbf{r}}$ is the electric dipole operator.

With the Wigner-Eckart theorem [9], the generic matrix element of the electric dipole operator can be simplified as

$$\langle F; m_F | \hat{\mathbf{d}} | F'; m_{F'} \rangle = \left[-\frac{1}{\sqrt{2}} Q(F, m_F; F', m_{F'}; J, J'; q = 1) + \frac{1}{\sqrt{2}} Q(F, m_F; F', m_{F'}; J, J'; q = -1) \right] d_e, \quad (7)$$

where $d_e = \langle 5S_{1/2} || er || 5P_{1/2} \rangle$ is the reduced matrix element ($d_e = 3 \times 10^{-29}$ C m for ^{87}Rb D_1 line) and $Q(F, m_F; F', m_{F'}; J, J'; q)$ is defined as

$$Q(F, m_F; F', m_{F'}; J, J'; q) \equiv (-1)^{F-m_F+F'+J+I+1} \sqrt{(2F+1)(2F'+1)} \times \begin{pmatrix} F & 1 & F' \\ -m_F & q & m_{F'} \end{pmatrix} \begin{Bmatrix} F & 1 & F' \\ J' & I & J \end{Bmatrix}. \quad (8)$$

The coefficients in round and in curly brackets are the 3- j and 6- j symbols, respectively.

It is then possible to define a laser Rabi frequency ω_R and a laser pumping rate Γ_p ,

$$\omega_R = \frac{\langle 5S_{1/2} || er || 5P_{1/2} \rangle E_0}{\hbar}, \quad (9)$$

$$\Gamma_p = \frac{\omega_R^2}{2\Gamma^*}. \quad (10)$$

In Eq. (10), Γ^* is the relaxation rate of the excited state; in particular, since the relaxation from the excited state is dominated by buffer gas collisions, we assume equal probability for the laser pumped atoms to fall into any of the ground-state sublevels.

Concerning the optical coherences excited by the laser, we assume that they can be written as

$$\rho_{\mu,m} = \delta_{\mu,m} e^{i(\omega_L t - k_L z)}, \quad (11)$$

where $\delta_{\mu,m}$ is a slowly function of time and with $\mu=4-8$ and $m=9, 10, 11$.

We assume at the moment $\phi \ll \Gamma^*$, which is a laser linewidth much narrower than the homogeneous linewidth of the optical transitions, a typical operating condition when distributed feedback (DFB) lasers or extended cavity lasers (ECL) are used.

We observe that according to the scheme of Fig. 2, also Zeeman coherences are excited in the ground state; in particular, the coupling laser induces Λ -type transitions exciting therefore the coherences $\rho_{46}, \rho_{68}, \rho_{57}$; for these coherences, we find a solution of the form $\rho_{46} = \delta_{46}$ and similarly for ρ_{68} and ρ_{57} . The second-order coherences, such as δ_{48}, δ_{49} , and $\delta_{8,11}$, have been neglected.

The nonresonant coupling of the laser field with the states $|1\rangle$, $|2\rangle$, and $|3\rangle$ is neglected, in fact it leads to the off-resonance light-shift, which is negligible in the POP operation.

To write explicitly the equations, we use the rotating-wave approximation to neglect the rapidly varying terms, and the adiabatic approximation to express the optical populations and coherences in terms of populations and coherences of the ground state.

B. Interaction atom-microwave field: $\hat{H}_{\mu\nu}$

It is assumed that the externally applied microwave is resonant with the transition between levels $|2\rangle$ and $|6\rangle$. The only matrix elements involved in this interaction are then ρ_{22} , ρ_{66} , and ρ_{26} . The microwave coherence oscillates at the frequency ω_0 of the applied rf field and is then set equal to $\rho_{26} = \delta_{26} e^{i\omega_0 t}$. We can associate a Rabi frequency $\tilde{b}_e = b_e e^{i\phi_e}$ to this field, with

$$b_e(r, z) = \frac{\mu_B \mu_0}{\hbar} H_z(r, z), \quad (12)$$

where μ_B is the Bohr magneton. In Eq. (12), the field $H_z(r, z)$ is proportional to the eigenvector cavity mode $H_{az}(r, z)$. In the case of the TE_{011} mode that has a well-defined component along the z axis (laser propagation axis), the eigenvector in cylindrical coordinates can be written as

$$H_{az}(r, z) = \sqrt{\frac{\eta'}{V_a}} J_0\left(\frac{x'_{01} r}{a}\right) \cos\left(\frac{\pi z}{d}\right). \quad (13)$$

In the previous equation, η' is the cavity filling factor [2,5], V_a is the volume of the cell, x'_{01} is the first root of the derivative of the Bessel function $J_0(x)$, and a and d are the radius and the length of the cavity, respectively. The phase ϕ_e is arbitrary.

C. ^{87}Rb buffer gas collisions: \hat{H}_{bg}

Following the approach reported in [5] (see also references therein), the Hamiltonian describing the interaction between alkali-metal atoms and buffer gas atoms or molecules can be written as

$$\hat{H}_{\text{bg}} = \delta A \mathbf{S} \cdot \mathbf{I} + \gamma \hbar \mathbf{S} \cdot \mathbf{N}. \quad (14)$$

The first term describes a modification of the hyperfine interaction between the alkali-metal electron spin \mathbf{S} and the nuclear spin \mathbf{I} taking place during the collision. This term is responsible for the well known pressure shift and broadening of the hyperfine line and for binary collisions leads to the so called Carver mechanism [10]. However, it does not produce any relaxation of the atomic populations and will be considered as a static perturbation in the following.

The second term is a spin-orbit (SO) type interaction between \mathbf{S} and the angular momentum of the colliding pair \mathbf{N} , where γ is a coupling constant; this interaction is depicted through the action of a random magnetic field $\mathbf{B}(t)$ coupling with \mathbf{S} (see [11]),

$$\hat{H}_{\text{bg}}^{\text{SO}} = -\gamma_S \hbar \mathbf{S} \cdot \mathbf{B}(t), \quad (15)$$

where γ_S is the electron gyromagnetic ratio.

To calculate the matrix elements of this Hamiltonian, it is more suitable to use the $\{|m_I, m_S\rangle\}$ representation where S_z is

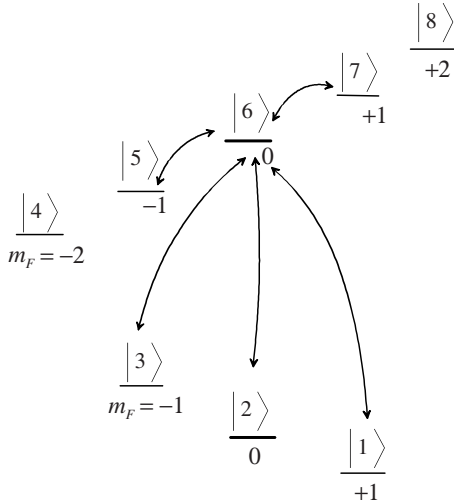


FIG. 3. Allowed transitions induced by the buffer gas Hamiltonian in the rate equations of ρ_{66} .

diagonal. The transition probabilities can be evaluated with a perturbation approach and it turns out that they are proportional to the Fourier transform of the correlation function of the random interaction [11]. It is then a straightforward calculation to see that the buffer gas induces selection rules among the ground-state sublevels: relaxation from a generic sublevel i does not take place with equal probability toward any other sublevel j [12]. For example, Fig. 3 shows the transitions involving the level $|6\rangle$. It can be observed that both hyperfine and Zeeman transitions can take place.

Explicit equations for the populations of the clock levels ρ_{22} and ρ_{66} , for their difference, and for the microwave coherence excited between them are given in [5]. It turns out that the equation for the population difference evolves in an uncoupled way from the other sublevels, and the system is in practice reduced again to a three-level approximation. However, this is not our case since according to the scheme of Fig. 2 the level $|6\rangle$ is coupled to other ground-state sublevels through the laser field. Moreover, the relaxation times induced by the buffer gas are of the same order of magnitude of the duration of the optical pumping phase, therefore laser pumping and buffer gas dynamics are mutually influenced. We then need to consider the equations for all the ground-state Zeeman sublevels.

Recently it has been demonstrated that with some buffer gases (typically Ar and Kr), the formation of van der Waals molecules can lead to frequency shifts of the microwave resonances dependent on the buffer gas pressure P in a non-linear way [13]. However, at the buffer gas pressures usually adopted in frequency standard applications (tens of Torr) and for buffer gas mixtures of N_2 and Ar, the formation of molecule Rb buffer gas gives rise to relaxation rates much smaller than those due to other relaxation mechanisms and therefore we will assume that only binary collisions take place. In this case, the relaxation rates are linear with P .

Coming to the excited state, buffer gas collisions cause a homogeneous broadening of the optical resonance that has been considered in the definition of the pumping rate through the term Γ^* , and also a redshift of the absorption line that

should be taken into account in the stabilization of the laser frequency.

D. ^{87}Rb - ^{87}Rb spin-exchange collisions: \hat{H}_{se}

Spin exchange is a well known and widely studied phenomenon. It is also of great interest in the field of vapor cell clocks, where it becomes the main relaxation mechanism for high atomic densities while at low temperatures spin exchange can be neglected with respect to buffer gas collisions and diffusion. The spin-exchange equations for the density matrix can be written taking into account the action of the spin-exchange operator on the evolution of $\hat{\rho}$ [5]. However, in [14] only the equations for the clock level difference $\rho_{66} - \rho_{22}$ and for the coherence excited between them are made explicit. But similarly to the previous case, the simultaneous presence of the laser field causes the time evolution of the clock levels coupled to the other Zeeman sublevels. Therefore, here the equations have been extended again to all the sublevels of the Zeeman manifold.

E. The Maxwell equations

As mentioned above, Eq. (2) leads to the Slater equation for the field sustained in a maser cavity. This field is generated by the magnetization created in the ensemble by the combination of laser pumping and microwave interrogation and reacts back to the atoms through the cavity. To this field we can associate a (complex) microwave Rabi frequency that we call \tilde{b}_i and that can be written as [2]

$$\tilde{b}_i(t) = 2i\bar{k}e^{i\psi}H_{az}(r,z) \int_{V_a} \delta_{26}(r,z,t)H_{az}(r,z)dV. \quad (16)$$

In this equation, \bar{k} is defined as

$$\bar{k} = \frac{\mu_0\mu_B^2 Q_L n}{\hbar}, \quad (17)$$

Q_L being the loaded cavity quality factor and n the atomic density.

The reduced cavity detuning ψ is defined as

$$\psi = 2Q_L \frac{\Delta\omega_c}{\omega_{26}}, \quad (18)$$

$\Delta\omega_c = \omega_c - \omega_{26}$ being the cavity detuning; it is assumed that $\psi \ll 1$.

Concerning Eq. (3), we note that the macroscopic polarization excited in the medium is defined as

$$P = n\text{Tr}(\hat{\rho}\hat{\mathbf{d}}). \quad (19)$$

Using Eq. (7), it is easy to calculate the non-null elements of the dipole moment operator, and Eq. (19) gives

$$P = nd_e e^{i(\omega_L t - kz)} \left[\frac{1}{2\sqrt{2}}\delta_{4,11} + \frac{1}{4}\delta_{5,10} + \frac{1}{4\sqrt{3}}\delta_{69} - \frac{1}{4\sqrt{3}}\delta_{6,11} - \frac{1}{4}\delta_{7,10} - \frac{1}{2\sqrt{2}}\delta_{89} \right] + \text{c.c.} \quad (20)$$

On the other hand, neglecting higher harmonics, the polarization can be written also as

$$P = \frac{1}{2} \tilde{P} e^{i(\omega_L t - kz)} + \text{c.c.}, \quad (21)$$

where \tilde{P} is a complex slowly varying function of position and time. From the two previous equations, it turns out that

$$\tilde{P} = nd_e \left[\frac{1}{\sqrt{2}} \delta_{4,11} + \frac{1}{2} \delta_{5,10} + \frac{1}{2\sqrt{3}} \delta_{69} - \frac{1}{2\sqrt{3}} \delta_{6,11} - \frac{1}{2} \delta_{7,10} - \frac{1}{\sqrt{2}} \delta_{89} \right]. \quad (22)$$

In terms of the Rabi frequency, the Maxwell equation becomes [15]

$$\frac{\partial \omega_R}{\partial z} + \frac{1}{c} \frac{\partial \omega_R}{\partial t} = \frac{\omega_L d_e}{2\epsilon_0 \hbar c} \text{Im} \tilde{P}, \quad (23)$$

where ϵ_0 is the vacuum permittivity and Im stands for imaginary part. The optical coherences of Eq. (22) can be expressed in terms of populations and coherences of the ground state thanks to the adiabatic approximation, so the Maxwell equation can be written as

$$\frac{\partial \omega_R}{\partial z} + \frac{1}{c} \frac{\partial \omega_R}{\partial t} = - \frac{\omega_L d_e^2 n}{24 \Gamma^* \epsilon_0 \hbar c} [6(\rho_{44} + \rho_{88}) + 3(\rho_{55} + \rho_{77}) + 2\rho_{66} - 2\sqrt{6}(\delta_{46}^r + \delta_{68}^r) - 6\delta_{57}^r]. \quad (24)$$

F. The complete system of Maxwell-Bloch equations

Taking into account all the considerations so far discussed, we can write down the complete set of equations describing the POP clock dynamics. As a consequence of the symmetry of the atomic levels configuration and of the excitation scheme shown in Fig. 2, the equations are symmetric for the simultaneous change of the following elements:

$$\begin{aligned} \rho_{11} &\rightarrow \rho_{33}, \\ \rho_{44} &\rightarrow \rho_{88}, \\ \rho_{55} &\rightarrow \rho_{77}, \\ \delta_{46} &\rightarrow \delta_{68}. \end{aligned} \quad (25)$$

If we make the assumption that at $t=0$ the atomic system is in thermal equilibrium ($\rho_{\mu\mu}=1/8$ and all the coherences are zero), the previous relations become identities that are satisfied at any time and allow us to reduce the total number of coupled equations. Therefore, the explicit form of the system (1)–(3) is given by the following set of coupled differential equations:

$$\begin{aligned} \frac{\partial \rho_{11}}{\partial t} &= D\nabla^2 \rho_{11} + (\gamma_{1c} + \gamma_{1se}) \frac{1}{16} (-13\rho_{11} + 4\rho_{44} + \rho_{55} + 1) \\ &+ \frac{\Gamma_p}{16} \left(\rho_{44} + \frac{1}{2}\rho_{55} + \frac{1}{6}\rho_{66} \right) - \frac{\Gamma_p}{16} \left(\frac{2\delta_{46}^r}{\sqrt{6}} + \frac{\delta_{57}^r}{2} \right), \end{aligned}$$

$$\rho_{22} = 1 - 2\rho_{11} - 2\rho_{44} - 2\rho_{55} - \rho_{66} \text{ for each } t,$$

$$\begin{aligned} \frac{\partial \rho_{44}}{\partial t} &= D\nabla^2 \rho_{44} + \frac{1}{8} (\gamma_{1c} + \gamma_{1se}) (-4\rho_{44} + 3\rho_{11} + \rho_{55}) \\ &+ \frac{\Gamma_p}{16} \left(-3\rho_{44} + \frac{1}{2}\rho_{55} + \frac{1}{6}\rho_{66} \right) + \frac{\Gamma_p}{16} \left(\frac{2}{\sqrt{6}} \delta_{46}^r - \frac{1}{2} \delta_{57}^r \right), \end{aligned}$$

$$\begin{aligned} \frac{\partial \rho_{55}}{\partial t} &= D\nabla^2 \rho_{55} + \frac{1}{16} (\gamma_{1c} + \gamma_{1se}) (-17\rho_{55} - 3\rho_{11} - 4\rho_{44} + 3) \\ &+ \frac{\Gamma_p}{16} \left(\rho_{44} - \frac{3}{2}\rho_{55} + \frac{1}{6}\rho_{66} \right) - \frac{\Gamma_p}{16} \left(\frac{2\delta_{46}^r(t)}{\sqrt{6}} - \frac{3}{2} \delta_{57}^r \right), \end{aligned}$$

$$\begin{aligned} \frac{\partial \rho_{66}}{\partial t} &= D\nabla^2 \rho_{66} + \frac{1}{8} (\gamma_{1c} + \gamma_{1se}) (-8\rho_{66} - 3\rho_{11} - 4\rho_{44} - \rho_{55} + 2) \\ &+ \frac{\Gamma_p}{16} \left(\rho_{44} + \frac{1}{2}\rho_{55} - \frac{7}{6}\rho_{66} \right) + \frac{\Gamma_p}{16} \left(\sqrt{6} \delta_{46}^r(t) - \frac{\delta_{57}^r}{2} \right) \\ &- \text{Im}(\tilde{b}_e^* \delta_{26}) - \text{Im}(\tilde{b}_i^* \delta_{26}), \end{aligned}$$

$$\begin{aligned} \frac{\partial \delta_{26}}{\partial t} &= D\nabla^2 \delta_{26} - \left[\gamma_{2c} + \gamma_{1se} \left(\frac{3}{8}\rho_{11} + \frac{1}{2}\rho_{44} + \frac{1}{8}\rho_{55} + \frac{1}{2} \right) + \frac{\Gamma_p}{24} \right. \\ &+ i\Omega_\mu + \frac{i}{4} k_{se} (2\rho_{11} + 2\rho_{44} + 2\rho_{55} + 2\rho_{66} - 1) \left. \right] \delta_{26} \\ &+ \frac{i}{2} (\tilde{b}_e + \tilde{b}_i) (2\rho_{11} + 2\rho_{44} + 2\rho_{55} + 2\rho_{66} - 1), \end{aligned}$$

$$\begin{aligned} \frac{\partial \delta_{46}^r}{\partial t} &= D\nabla^2 \delta_{46}^r - \left[\frac{3}{4} (\gamma_{1c} + \gamma_{1se}) + \frac{7}{48} \Gamma_p \right] \delta_{46}^r \\ &- \left(\frac{\gamma_{1c} \tau \omega_z}{16} + 2\omega_z \right) \delta_{46}^i + \frac{1}{8} \sqrt{\frac{3}{2}} (\gamma_{1c} + \gamma_{1se}) \delta_{57}^r \\ &+ \frac{\Gamma_p}{8\sqrt{6}} (\rho_{44} + \rho_{66}), \end{aligned}$$

$$\begin{aligned} \frac{\partial \delta_{46}^i}{\partial t} &= D\nabla^2 \delta_{46}^i - \left[\frac{3}{4} (\gamma_{1c} + \gamma_{1se}) + \frac{7}{48} \Gamma_p \right] \delta_{46}^i \\ &+ \left(\frac{\gamma_{1c} \tau \omega_z}{16} + 2\omega_z \right) \delta_{46}^r + \frac{1}{8} \sqrt{\frac{3}{2}} (\gamma_{1c} + \gamma_{1se}) \delta_{57}^i, \end{aligned}$$

$$\begin{aligned} \frac{\partial \delta_{57}^r}{\partial t} &= D\nabla^2 \delta_{57}^r - \left[\frac{13}{16} (\gamma_{1c} + \gamma_{1se}) + \frac{\Gamma_p}{8} \right] \delta_{57}^r \\ &- \left(\frac{\gamma_{1c} \tau \omega_z}{16} + 2\omega_z \right) \delta_{57}^i + \frac{1}{4} \sqrt{\frac{3}{2}} (\gamma_{1c} + \gamma_{1se}) \delta_{46}^r \\ &+ \frac{\Gamma_p}{8} \rho_{55}, \end{aligned}$$

$$\frac{\partial \delta_{57}^i}{\partial t} = D\nabla^2 \delta_{57}^i - \left[\frac{13}{16}(\gamma_{1c} + \gamma_{1se}) + \frac{\Gamma_p}{8} \right] \delta_{57}^i + \left(\frac{\gamma_{1c} \tau \omega_z}{16} + 2\omega_z \right) \delta_{57}^r + \frac{1}{4} \sqrt{\frac{3}{2}} (\gamma_{1c} + \gamma_{1se}) \delta_{46}^i,$$

$$\tilde{b}_i(t) = 2ike^{i\psi} H_{az}(r, z) \int_{V_a} \delta_{26}(r, z, t) H_{az}(r, z) dV,$$

$$\frac{\partial \omega_R}{\partial z} + \frac{1}{c} \frac{\partial \omega_R}{\partial t} = - \frac{\omega_L d_e^2 n}{24\Gamma^* \epsilon_0 \hbar c} \times [6\rho_{44} + 3\rho_{55} + \rho_{66} - 2\sqrt{6}\delta_{46}^r - 3\delta_{57}^r]. \quad (26)$$

It is of course understood that all populations and coherences are functions of time and of the spatial variables. Besides the approximations already mentioned, this set of equations has been obtained also according to the following assumptions widely satisfied in our physical situation:

$$\begin{aligned} \omega_R &\ll \Gamma^*, \\ b_e, |\tilde{b}_i| &\ll \Gamma^*, \\ \Omega_\mu &\ll \Gamma^*, \end{aligned} \quad (27)$$

Ω_μ being the microwave detuning $\omega_0 - \omega_{26}$. In Eq. (26), δ_{ab}^r (δ_{ab}^i) stands for the real (imaginary) part of δ_{ab} .

In the previous equations, γ_{1c} and γ_{2c} are the relaxation rates of populations and hyperfine coherence due to the buffer gas interaction and are given, respectively, by

$$\begin{aligned} \gamma_{1c} &= L_0 \bar{v}_{r, \text{bg}} \sigma_1 \frac{P}{P_0}, \\ \gamma_{2c} &= L_0 \bar{v}_{r, \text{bg}} \sigma_2 \frac{P}{P_0}, \end{aligned} \quad (28)$$

where L_0 is Loschmidt's constant, $\bar{v}_{r, \text{bg}}$ is the relative average velocity Rb buffer gas, and σ_1 and σ_2 are the Rb buffer gas cross sections.

Concerning the relaxation produced by spin exchange, we observe that in the equation for the hyperfine coherence, there is a term proportional to k_{se} that is defined as

$$k_{se} = \bar{v}_r \lambda_{ex} n, \quad (29)$$

where \bar{v}_r is the average relative velocity of the colliding Rb atoms ($\bar{v}_r \approx 385$ m/s) and λ_{ex} is a cross section responsible for a small spin-exchange shift that has been analyzed in some detail in [16]; in the present context, it is not important and will be neglected in the following. We also note that the term proportional to γ_{1se} in the equation for δ_{26} is a very slowly varying function of time and with a good approximation can be assimilated to a constant equal to $\frac{5}{8}$. Therefore, for the spin-exchange relaxation rate of the coherence γ_{2se} the well known relation [5]

$$\gamma_{2se} = \frac{6I + 1}{8I + 4} = \frac{5}{8} \gamma_{1se} \quad (30)$$

is satisfied for ^{87}Rb . In the previous equation, γ_{1se} is defined as usual as

$$\gamma_{1se} = \bar{v}_r \sigma_{ex} n, \quad (31)$$

where σ_{ex} is the spin-exchange cross section responsible for the broadening of the resonance line ($\sigma_{ex} \approx 1.6 \times 10^{-14}$ cm² for ^{87}Rb [5,16]).

In the equations of the Zeeman coherences, τ is the time duration of the rubidium buffer gas collision and for binary collisions it is of the order of 10^{-12} s. By an “*a posteriori*” computation, it turns out that for values sufficiently higher than ω_z , the role played by the coherences becomes negligible. This is expected since ω_z is proportional to B_0 and the maximum of coherence occurs for $B_0=0$, where the Zeeman levels are degenerate (Hanle effect [17]). For typical values of the relaxation rates (see later), it turns out that for $\omega_z/2\pi \gg 1$ kHz the interference terms are averaged out and the coherences can be neglected. So the system (26) further simplifies,

$$\begin{aligned} \frac{\partial \rho_{11}}{\partial t} &= D\nabla^2 \rho_{11} + \frac{1}{16} (\gamma_{1c} + \gamma_{1se}) (-13\rho_{11} + 4\rho_{44} + \rho_{55} + 1) \\ &\quad + \frac{\Gamma_p}{16} \left(\rho_{44} + \frac{1}{2}\rho_{55} + \frac{1}{6}\rho_{66} \right), \end{aligned}$$

$$\begin{aligned} \frac{\partial \rho_{44}}{\partial t} &= D\nabla^2 \rho_{44} + \frac{1}{8} (\gamma_{1c} + \gamma_{1se}) (3\rho_{11} - 4\rho_{44} + \rho_{55}) \\ &\quad + \frac{\Gamma_p}{16} \left(-3\rho_{44} + \frac{1}{2}\rho_{55} + \frac{1}{6}\rho_{66} \right), \end{aligned}$$

$$\begin{aligned} \frac{\partial \rho_{55}}{\partial t} &= D\nabla^2 \rho_{55} - \frac{1}{16} (\gamma_{1c} + \gamma_{1se}) (3\rho_{11} + 4\rho_{44} + 17\rho_{55} - 3) \\ &\quad + \frac{\Gamma_p}{16} \left(\rho_{44} - \frac{3}{2}\rho_{55} + \frac{1}{6}\rho_{66} \right), \end{aligned}$$

$$\begin{aligned} \frac{\partial \rho_{66}}{\partial t} &= D\nabla^2 \rho_{66} - (\gamma_{1c} + \gamma_{1se}) \rho_{66} - \frac{1}{8} (\gamma_{1c} + \gamma_{1se}) (3\rho_{11} + 4\rho_{44} \\ &\quad + \rho_{55} - 2) + \frac{\Gamma_p}{16} \left(\rho_{44} + \frac{1}{2}\rho_{55} - \frac{7}{6}\rho_{66} \right) - \text{Im}(\tilde{b}_e^* \delta_{26}) \\ &\quad - \text{Im}(\tilde{b}_i^* \delta_{26}), \end{aligned}$$

$$\begin{aligned} \frac{\partial \Delta}{\partial t} &= D\nabla^2 \Delta - (\gamma_{1c} + \gamma_{1se}) \Delta - \frac{\Gamma_p}{12} \rho_{66} - 2 \text{Im}(\tilde{b}_e^* \delta_{26}) \\ &\quad - 2 \text{Im}(\tilde{b}_i^* \delta_{26}), \end{aligned}$$

$$\begin{aligned} \frac{\partial \delta_{26}}{\partial t} &= D\nabla^2 \delta_{26} - \left[\gamma_{2c} + \gamma_{2se} + \frac{\Gamma_p}{24} + i \left(\Omega_\mu - \frac{k_{se}}{4} \Delta \right) \right] \delta_{26} \\ &\quad + \frac{i}{2} (\tilde{b}_e + \tilde{b}_i) \Delta, \end{aligned}$$

$$\tilde{b}_i(t) = 2ike^{i\psi} H_{az}(r, z) \int_{V_a} \delta_{26}(r, z, t) H_{az}(r, z) dV,$$

$$\frac{\partial \Gamma_p}{\partial z} + \frac{1}{c} \frac{\partial \Gamma_p}{\partial t} = -\frac{\alpha}{\Gamma^*} \Gamma_p \frac{6\rho_{44} + 3\rho_{55} + \rho_{66}}{12}. \quad (32)$$

The Maxwell equation for the electric field amplitude has been written in terms of the pumping rate defined in Eq. (10), α being the linear absorption coefficient defined as

$$\alpha = \frac{\omega_L d_e^2 n}{\epsilon_0 \hbar c}. \quad (33)$$

In Eqs. (32), we have substituted the equation for ρ_{22} (trace equation) with the equivalent equation for the population difference (Δ) between the clock levels,

$$\Delta \equiv \rho_{66} - \rho_{22} = 2(\rho_{11} + \rho_{44} + \rho_{55} + \rho_{66}) - 1. \quad (34)$$

Equations (32) will be numerically solved in a cylindrical coordinate system with origin in the center of the cell. Due to the symmetry around the z axis, there is no dependence on the angular variable ϕ in the Laplacian operator. The following boundary conditions for populations and coherence have been used:

$$\rho_{\mu\mu}(r=R, z, t) = \frac{1}{8}, \quad \mu = 1, 4, 5, 6,$$

$$\rho_{\mu\mu}(r, z=-L/2, t) = \rho_{\mu\mu}(r, z=L/2, t) = \frac{1}{8},$$

$$\left. \frac{\partial \rho_{\mu\mu}(r, z, t)}{\partial r} \right|_{r=0} = 0,$$

$$\Delta(r=R, z, t) = 0,$$

$$\Delta(r, z=-L/2, t) = \Delta(r, z=L/2, t) = 0,$$

$$\left. \frac{\partial \Delta(r, z, t)}{\partial r} \right|_{r=0} = 0,$$

$$\delta_{26}(r=R, z, t) = 0,$$

$$\delta_{26}(r, z=-L/2, t) = \delta_{26}(r, z=L/2, t) = 0,$$

$$\left. \frac{\partial \delta_{26}(r, z, t)}{\partial r} \right|_{r=0} = 0. \quad (35)$$

These boundary conditions are dictated by the assumption of complete relaxation on the walls of the cell and are common to all the POP operation phases and then will not be reported in the following for the sake of brevity.

Numerical solutions of the coupled equations (32) with boundary conditions (35) will be provided in the following section.

We still remark here on an important feature of the POP operation: when $\Gamma_p=0$ (laser off), as during the Ramsey in-

teraction time, the equations for Δ , for δ_{26} , and for \tilde{b}_i are uncoupled from the other equations. This means that when the clock transition takes place, the atoms can be assimilated to a two-level system: $|2\rangle$ and $|6\rangle$. Other atomic levels play a role only during the optical pumping phase and during the detection time when the optical transmission signal is used to observe the clock transition. This feature, not present of course in continuous operation, is of basic importance to achieve high-frequency stability performances [4].

III. NUMERICAL ANALYSIS

In this section, we report the numerical solutions of Eqs. (32) as obtained for a typical POP operation cycle. We will refer in the following to a cell of length $L=1.8$ cm and radius $R=1.5$ cm containing the ^{87}Rb atoms and filled with a buffer gas mixture of Ar and N_2 at the total pressure of 25 Torr and with a pressure ratio $P(\text{Ar})/P(\text{N}_2)=1.6$. From definitions (5) and (28) and from the values reported in the literature [5], γ_{1c} and γ_{2c} can be assumed equal to

$$\gamma_{1c} = 12 \text{ s}^{-1},$$

$$\gamma_{2c} = 102 \text{ s}^{-1} \quad (36)$$

while the diffusion constant D turns out to be

$$D = 8 \text{ cm}^2/\text{s}. \quad (37)$$

The relaxation rate of the excited state is

$$\Gamma^* = 3 \times 10^9 \text{ s}^{-1}. \quad (38)$$

Concerning the spin-exchange relaxation rates, we will analyze two different physical situations: a low-temperature regime (that implies a low atomic density) and a high-temperature regime (high atomic density). In the first case, we will assume a working temperature of $T_0=36$ °C, corresponding to an atomic density of $n=3 \times 10^{10} \text{ cm}^{-3}$ and to an optical length of the cell $\zeta=\alpha L/\Gamma^* \approx 0.3$ (optically thin medium). In this case, we have

$$\gamma_{1se} = 18.5 \text{ s}^{-1},$$

$$\gamma_{2se} = 11 \text{ s}^{-1}. \quad (39)$$

In the high-temperature regime, we will consider $T_0=65$ °C, corresponding to an atomic density of $n=5 \times 10^{11} \text{ cm}^{-3}$ ($\zeta=5$), so we have

$$\gamma_{1se} = 307 \text{ s}^{-1},$$

$$\gamma_{2se} = 192 \text{ s}^{-1}. \quad (40)$$

We suppose to place the cell in a cylindrical microwave cavity of radius $a=2.9$ cm and length $d=3.7$ cm. The cell and the cavity are coaxial and with the same center. The loaded cavity quality factor is assumed to be $Q_L=10\,000$ and the filling factor $\eta'=0.4$; from Eq. (16), it turns out that \tilde{b}_i is proportional to $k=\eta'\bar{k}$, which is the so called gain factor, and has the meaning of a number of emitted microwave photons per second by each atom. From Eq. (17), we have

$$\begin{aligned}
 k &= 100 \text{ s}^{-1} \quad \text{at} \quad T_0 = 36 \text{ }^\circ\text{C}, \\
 k &= 2200 \text{ s}^{-1} \quad \text{at} \quad T_0 = 65 \text{ }^\circ\text{C}. \quad (41)
 \end{aligned}$$

At low temperature, the cavity feedback on the atoms is neglected in all the POP operation phases; this means neglecting \tilde{b}_i in the equations, while in the high-temperature regime the effect of the cavity feedback is fully taken into account only during the Ramsey time, being responsible of the cavity pulling that will be discussed later on.

We finally observe that although we investigate the POP operation defined by these parameters, Eqs. (32) are absolutely general and can be applied to the description of several different physical situations, including, of course, continuous rf-optical double resonance experiments.

A. Optical pumping

During the optical pumping phase, no microwave is externally applied to the atoms ($b_e=0$) and the previous set of equations becomes

$$\begin{aligned}
 \frac{\partial \rho_{11}^{\text{op}}}{\partial t} &= D\nabla^2 \rho_{11}^{\text{op}} + \frac{1}{16}(\gamma_{1c} + \gamma_{1\text{se}})(-13\rho_{11}^{\text{op}} + 4\rho_{44}^{\text{op}} + \rho_{55}^{\text{op}} + 1) \\
 &\quad + \frac{\Gamma_p}{16} \left(\rho_{44}^{\text{op}} + \frac{1}{2}\rho_{55}^{\text{op}} + \frac{1}{6}\rho_{66}^{\text{op}} \right), \\
 \frac{\partial \rho_{44}^{\text{op}}}{\partial t} &= D\nabla^2 \rho_{44}^{\text{op}} + \frac{1}{8}(\gamma_{1c} + \gamma_{1\text{se}})(3\rho_{11}^{\text{op}} - 4\rho_{44}^{\text{op}} + \rho_{55}^{\text{op}}) \\
 &\quad + \frac{\Gamma_p}{16} \left(-3\rho_{44}^{\text{op}} + \frac{1}{2}\rho_{55}^{\text{op}} + \frac{1}{6}\rho_{66}^{\text{op}} \right), \\
 \frac{\partial \rho_{55}^{\text{op}}}{\partial t} &= D\nabla^2 \rho_{55}^{\text{op}} - \frac{1}{16}(\gamma_{1c} + \gamma_{1\text{se}})(3\rho_{11}^{\text{op}} + 4\rho_{44}^{\text{op}} + 17\rho_{55}^{\text{op}} - 3) \\
 &\quad + \frac{\Gamma_p}{16} \left(\rho_{44}^{\text{op}} - \frac{3}{2}\rho_{55}^{\text{op}} + \frac{1}{6}\rho_{66}^{\text{op}} \right), \\
 \frac{\partial \rho_{66}^{\text{op}}}{\partial t} &= D\nabla^2 \rho_{66}^{\text{op}} - (\gamma_{1c} + \gamma_{1\text{se}})\rho_{66}^{\text{op}} \\
 &\quad - \frac{1}{8}(\gamma_{1c} + \gamma_{1\text{se}})(3\rho_{11}^{\text{op}} + 4\rho_{44}^{\text{op}} + \rho_{55}^{\text{op}} - 2) \\
 &\quad + \frac{\Gamma_p}{16} \left(\rho_{44}^{\text{op}} + \frac{1}{2}\rho_{55}^{\text{op}} - \frac{7}{6}\rho_{66}^{\text{op}} \right), \\
 \frac{\partial \Delta^{\text{op}}}{\partial t} &= D\nabla^2 \Delta^{\text{op}} - (\gamma_{1c} + \gamma_{1\text{se}})\Delta^{\text{op}} - \frac{\Gamma_p}{12}\rho_{66}^{\text{op}}, \\
 \frac{\partial \delta_{26}^{\text{op}}}{\partial t} &= D\nabla^2 \delta_{26}^{\text{op}} - \left[\gamma_{2c} + \gamma_{2\text{se}} + \frac{\Gamma_p}{24} + i \left(\Omega_\mu - \frac{k_{\text{se}}}{4} \Delta^{\text{op}} \right) \right] \delta_{26}^{\text{op}}, \\
 \frac{\partial \Gamma_p}{\partial z} + \frac{1}{c} \frac{\partial \Gamma_p}{\partial t} &= - \frac{\alpha}{\Gamma_p^*} \Gamma_p \frac{6\rho_{44}^{\text{op}} + 3\rho_{55}^{\text{op}} + \rho_{66}^{\text{op}}}{12}, \quad (42)
 \end{aligned}$$

where the superscript ‘‘op’’ indicates that the equations have been specified for the optical pumping phase. We initially

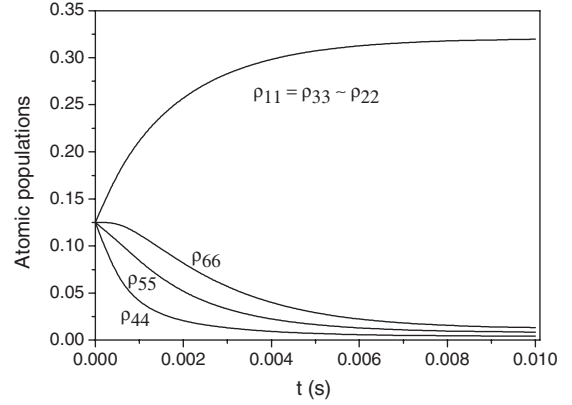


FIG. 4. Time behavior of the populations during the optical pumping phase; $\Gamma_p=10\,000 \text{ s}^{-1}$.

suppose that at $t=0$ the atoms are in thermal equilibrium, therefore no hyperfine coherence exists in the sample.

The following initial conditions for $t=0$ have to be used together with boundary conditions (35):

$$\begin{aligned}
 \rho_{\mu\mu}^{\text{op}}(r, z, t=0) &= \frac{1}{8}, \quad \mu = 1, 4, 5, 6, \\
 \Delta^{\text{op}}(r, z, t=0) &= 0, \\
 \delta_{26}^{\text{op}}(r, z, t=0) &= 0, \\
 \Gamma_p(r, z, t=0) &= \Gamma_{p0}, \quad (43)
 \end{aligned}$$

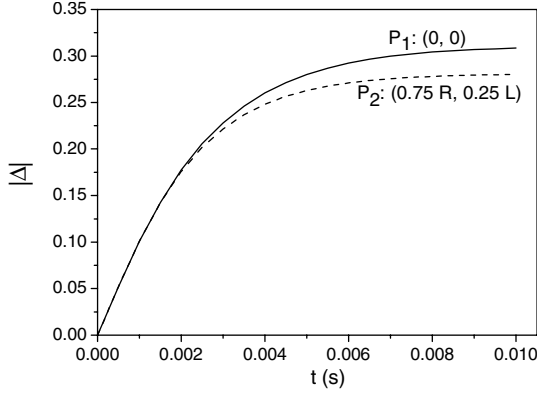
Γ_{p0} being the laser pumping rate at the entrance of the cell: $\Gamma_p(r, z=0, t) = \Gamma_{p0}$.

Figure 4 shows the time behavior of the atomic populations ρ_{11} , ρ_{44} , ρ_{55} , and ρ_{66} as calculated in the center of the cell in the case of the low-temperature regime.

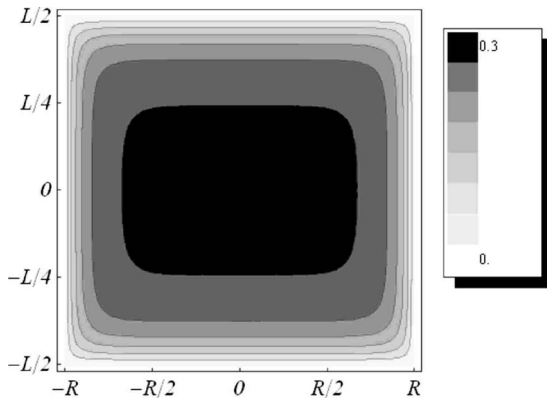
As expected, levels coupled to the laser are depleted and the atomic population is (almost) equally distributed among levels $|1\rangle$, $|2\rangle$, and $|3\rangle$.

Figure 5(a) shows the population inversion as calculated in the center of the cell (P_1) and in another point closer to the walls (P_2). The value of population inversion achieved in the two points is slightly different, so that the diffusion motion introduces a further nonuniformity to be added to other nonuniformity causes, mainly the laser absorption in the cell and the dependence of the microwave field on the spatial variables [see Eq. (13)]. Even though the measurement process of the observables performs a spatial average over the cell, these nonuniformity sources still remain and lead to a ‘‘positioning shift,’’ as will be shown later. Figure 5(b) shows the nonuniform distribution of population inversion in a median plane of the cell.

The previous transients have been calculated also in the case of an optically thick medium (high temperature) and similar behaviors have been obtained. However, in this case, spin-exchange becomes the predominant relaxation phenomenon: the atoms mainly relax due to spin-exchange collisions



(a)



(b)

FIG. 5. (a) Population inversion calculated in the center of the cell (continuous line) and in the point of coordinate: $r=0.75R$, $z=0.5L/2$ (dot line); $\Gamma_p=10\,000\text{ s}^{-1}$; (b) distribution of $|\Delta|$ at $t=0.01\text{ s}$ in the median plane of the cell.

before reaching the wall of the cell through the buffer gas, and with a good approximation we can make the following substitution in the equations:

$$D\nabla^2\rho_{\mu\mu} \rightarrow -\gamma_d\rho_{\mu\mu} + \frac{1}{8}\gamma_d, \quad (44)$$

γ_d being the relaxation rate related to the first diffusion mode defined as

$$\gamma_d = \left[\left(\frac{2.405}{R} \right)^2 + \left(\frac{\pi}{L} \right)^2 \right] D \quad (45)$$

that for our cell turns out $\gamma_d=45\text{ s}^{-1}$. In the high-density limit, the approximation (44) means to neglect the diffusion dynamics only very close to the walls of the cell.

It is important to point out that, independently on temperature regime, the optical pumping rate is slower than that calculated in a three-level approximation where the assumption of a zero nuclear spin is implicit. In fact, taking into account that each photon carries only one unit of angular momentum, when $I \neq 0$ many units of angular momentum are required to pump the atoms in all the sublevels [18].

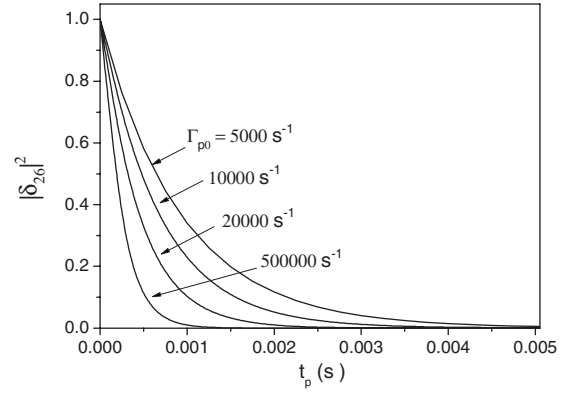


FIG. 6. Extinction of the coherence in the high-temperature regime for different laser pumping rates.

In principle, a non-null hyperfine coherence may be present at the beginning of the optical pumping phase. This coherence can be generated, for example, in previous operation cycles so that the system is not in thermal equilibrium at $t=0$. Figure 6 shows the time behavior of $|\delta_{26}(t)|^2$ for different laser pumping values in the case of high temperature; the approximation (44) has been applied also for the equation of δ_{26} in the form $D\nabla^2\delta_{26} \rightarrow -\gamma_d\delta_{26}$. The initial condition has been normalized so that $\delta_{26}(0)=1+i0$.

It can be observed that, as is well known, the laser pulse reduces the microwave coherence but, similarly to Fig. 5, the extinction rate is slower than that calculated in the three-level approach [4]. Anyway, when the laser pulse area satisfies the condition $\Gamma_{p0}t_p \gg 1$, no significant coherence is present at the beginning of a new cycle and we can say that consecutive cycles are disjoint from each other. If this condition is not satisfied, a recursive numerical approach is required in order to calculate the steady-state value of the residual coherence. However, supported also by our experiments, we will assume that the laser pulse, besides performing a large population inversion between the clock levels, is able to suppress any residual microwave coherence. The optical pumping and the subsequent interrogation phase are really uncoupled and a single cycle is well representative of the dynamics in which we are interested.

From Figs. 5 and 6, we can state that a pumping time $t_p \approx 4\text{ ms}$ and a pumping rate $\Gamma_{p0} \geq 10\,000\text{ s}^{-1}$ may represent a good experimental choice for the POP operation.

B. Microwave interrogation

After optical pumping, the atoms are interrogated with a first microwave pulse resonant with levels $|2\rangle$ and $|6\rangle$. This pulse lasts a time t_1 and can be chosen much shorter than all the relaxation rates we considered earlier. During this phase all the relaxations phenomena, including diffusion, are then neglected and we can say that during this very short time, the quantities ρ_{11} , ρ_{44} , and ρ_{55} do not evolve and the spatial variables are considered fixed (frozen). Equations (32) turn out ($\Gamma_p=0$) to be

$$\frac{\partial\rho_{11}^{\mu\nu}}{\partial t} = \frac{\partial\rho_{44}^{\mu\nu}}{\partial t} = \frac{\partial\rho_{55}^{\mu\nu}}{\partial t} = 0,$$

$$\begin{aligned}\frac{\partial \rho_{66}^{\mu w}}{\partial t} &= b_e \delta_{26}^{r, \mu w}, \\ \frac{\partial \Delta^{\mu w}}{\partial t} &= 2b_e \delta_{26}^{r, \mu w}, \\ \frac{\partial \delta_{26}^{\mu w}}{\partial t} &= -i \left(\Omega_\mu - \frac{k_{se}}{4} \Delta^{\mu w} \right) \delta_{26}^{\mu w} - \frac{b_e}{2} \Delta^{\mu w},\end{aligned}\quad (46)$$

where the quantities are now labeled by the index “ μw .” In the previous equations, the arbitrary phase ϕ_e has been set equal to $\pi/2$ and the feedback of the cavity on the atoms has been neglected since $b_e \gg |\tilde{b}_i^*|$.

As mentioned before, the clock dynamics is formally reduced to that of a two-level system described by Δ and δ_{26} ; the effect of the other sublevels is actually hidden in the initial conditions, which can be written as

$$\begin{aligned}\rho_{\mu\mu}^{\mu w}(r, z, t) &= \rho_{\mu\mu}^{\text{op}}(r, z, t_p) \quad \text{for } 0 \leq t \leq t_1, \quad \mu = 1, 4, 5, \\ \rho_{66}^{\mu w}(r, z, t=0) &= \rho_{66}^{\text{op}}(r, z, t_p), \\ \Delta^{\mu w}(r, z, t=0) &= \Delta^{\text{op}}(r, z, t_p) \equiv 2[\rho_{11}^{\text{op}}(r, z, t_p) + \rho_{44}^{\text{op}}(r, z, t_p) \\ &\quad + \rho_{55}^{\text{op}}(r, z, t_p) + \rho_{66}^{\text{op}}(r, z, t_p)] - 1, \\ \delta_{26}^{\mu w}(r, z, t=0) &= 0,\end{aligned}\quad (47)$$

where now for $t=0$ we mean the beginning of the microwave interrogation phase. The solution of the previous equations for $\Delta^{\mu w}$ and $\delta_{26}^{\mu w}$ is well known (see, for example, [4]) and can be expressed in terms of the Bloch vector of components $(\delta_{26}^{r, \mu w}, \delta_{26}^{i, \mu w}, \Delta^{\mu w})$,

$$\begin{aligned}\delta_{26}^{r, \mu w}(r, z, t_1) &= -\frac{b_e(r, z)}{2\xi(r, z)} \sin[\xi(r, z)t_1] \Delta^{\text{op}}(r, z, t_p), \\ \delta_{26}^{i, \mu w}(r, z, t_1) &= \frac{\Omega_\mu b_e(r, z)}{2\xi(r, z)^2} \{1 - \cos[\xi(r, z)t_1]\} \Delta^{\text{op}}(r, z, t_p), \\ \Delta^{\mu w}(r, z, t_1) &= \frac{\Omega_\mu^2 + b_e(r, z)^2 \cos[\xi(r, z)t_1]}{\xi(r, z)^2} \Delta^{\text{op}}(r, z, t_p),\end{aligned}\quad (48)$$

where $\xi(r, z) = \sqrt{b_e^2(r, z) + \Omega_\mu^2}$. The trace condition can easily provide $\rho_{66}^{\mu w}$. To this result, we can give a physical interpretation: at the end of the microwave pulse, the amount of hyperfine coherence in a certain point of the cell is proportional to the population inversion generated in that point at the end of the pumping phase.

The free decay region between the two microwave pulses is described by the following system obtained from Eqs. (32) with $\Gamma_p=0$ and $b_e=0$:

$$\begin{aligned}\frac{\partial \rho_{11}^{\text{free}}}{\partial t} &= D\nabla^2 \rho_{11}^{\text{free}} + \frac{1}{16}(\gamma_{1c} + \gamma_{1se}) \\ &\quad \times (-13\rho_{11}^{\text{free}} + 4\rho_{44}^{\text{free}} + \rho_{55}^{\text{free}} + 1),\end{aligned}$$

$$\frac{\partial \rho_{44}^{\text{free}}}{\partial t} = D\nabla^2 \rho_{44}^{\text{free}} + \frac{1}{8}(\gamma_{1c} + \gamma_{1se})(3\rho_{11}^{\text{free}} - 4\rho_{44}^{\text{free}} + \rho_{55}^{\text{free}}),$$

$$\begin{aligned}\frac{\partial \rho_{55}^{\text{free}}}{\partial t} &= D\nabla^2 \rho_{55}^{\text{free}} - \frac{1}{16}(\gamma_{1c} + \gamma_{1se}) \\ &\quad \times (3\rho_{11}^{\text{free}} + 4\rho_{44}^{\text{free}} + 17\rho_{55}^{\text{free}} - 3),\end{aligned}$$

$$\begin{aligned}\frac{\partial \rho_{66}^{\text{free}}}{\partial t} &= D\nabla^2 \rho_{66}^{\text{free}} - (\gamma_{1c} + \gamma_{1se})\rho_{66}^{\text{free}} - \frac{1}{8}(\gamma_{1c} + \gamma_{1se}) \\ &\quad \times (3\rho_{11}^{\text{free}} + 4\rho_{44}^{\text{free}} + \rho_{55}^{\text{free}} - 2) - \mathcal{J}(\tilde{b}_i^* \delta_{26}^{\text{free}}),\end{aligned}$$

$$\frac{\partial \Delta^{\text{free}}}{\partial t} = D\nabla^2 \Delta^{\text{free}} - (\gamma_{1c} + \gamma_{1se})\Delta^{\text{free}} - 2\mathcal{J}(\tilde{b}_i^* \delta_{26}^{\text{free}}),$$

$$\begin{aligned}\frac{\partial \delta_{26}^{\text{free}}}{\partial t} &= D\nabla^2 \delta_{26}^{\text{free}} - \left[\gamma_{2c} + \gamma_{2se} + i \left(\Omega_\mu - \frac{k_{se}}{4} \Delta^{\text{free}} \right) \right] \delta_{26}^{\text{free}} \\ &\quad + \frac{i}{2} \tilde{b}_i \Delta^{\text{free}},\end{aligned}$$

$$\tilde{b}_i(t) = 2ike^{i\psi} H_{a_z}(r, z) \int_{V_a} \delta_{26}^{\text{free}}(r, z, t) H_{a_z}(r, z) dV. \quad (49)$$

It is now important to distinguish between the two regimes of low and high atomic density; in the first case, the diffusion is taken into account explicitly and the feedback of the cavity on the atoms is neglected ($\tilde{b}_i=0$). It is then possible to give a formal expression for Δ^{free} and $\delta_{26}^{\text{free}}$ by solving the diffusion equation [19].

For the population inversion, we obtain

$$\begin{aligned}\Delta^{\text{free}}(r, z, t) &= \sum_{i,j} \Theta_{i,j} e^{-(\gamma_{1c} + \gamma_{1se}) + D(\mu_i^2 + \nu_j^2)t} J_0(\mu_i r) \\ &\quad \times \cos\left[\frac{(2j+1)\pi z}{L}\right],\end{aligned}\quad (50)$$

where the coefficients $\Theta_{i,j}$ are given by

$$\begin{aligned}\Theta_{i,j} &= \frac{4}{LR^2 J_1^2(x_{0i})} \int_{-L/2}^{L/2} \int_0^R r dr dz [\Delta^{\mu w}(r, z, t_1)] J_0\left(\frac{x_{0i} r}{R}\right) \\ &\quad \times \cos\left[\frac{(2j+1)\pi z}{L}\right].\end{aligned}\quad (51)$$

In Eqs. (50) and (51), $\mu_i = \frac{x_{0i}}{R}$, x_{0i} being the i th root of $J_0(x)$ and $\nu_j = \frac{(2j+1)\pi}{L}$.

For the microwave coherence, a similar solution is found,

$$\begin{aligned}\delta_{26}^{\text{free}}(r, z, t) &= e^{-i\Omega_\mu t} \sum_{i,j} A_{i,j} e^{-(\gamma_{1c} + \gamma_{1se}) + D(\mu_i^2 + \nu_j^2)t} J_0(\mu_i r) \\ &\quad \times \cos\left[\frac{(2j+1)\pi z}{L}\right],\end{aligned}\quad (52)$$

where $A_{i,j} = B_{i,j} + iC_{i,j}$ with

$$B_{i,j} = \frac{4}{LR^2 J_1^2(x_{0i})} \int_{-L/2}^{L/2} \int_0^R r dr dz [\delta_{26}^{r,\mu w}(r,z,t_1)] J_0\left(\frac{x_{0i} r}{R}\right) \times \cos\left[\frac{(2j+1)\pi z}{L}\right], \quad (53)$$

$$C_{i,j} = \frac{4}{LR^2 J_1^2(x_{0i})} \int_{-L/2}^{L/2} \int_0^R r dr dz [\delta_{26}^{i,\mu w}(r,z,t_1)] J_0\left(\frac{x_{0i} r}{R}\right) \times \cos\left[\frac{(2j+1)\pi z}{L}\right]. \quad (54)$$

Assuming that the atoms evolve freely for a time T , it is possible to evaluate $\Delta^{\text{free}}(r,z,T)$ and $\delta_{26}^{\text{free}}(r,z,T)$, which are the initial conditions for the second microwave pulse that is identified by the superscript $(2)\mu w$,

$$\Delta^{(2)\mu w}(r,z,t=0) = \Delta^{\text{free}}(r,z,T),$$

$$\delta_{26}^{(2)\mu w}(r,z,t=0) = \delta_{26}^{\text{free}}(r,z,T). \quad (55)$$

The following equations provide the expressions of Δ and δ_{26} at the end of the second microwave pulse:

$$\begin{aligned} \delta_{26}^{r,(2)\mu w}(r,z,t_1) &= \cos[\xi(r,z)t_1] \delta_{26}^{r,\text{free}}(r,z,T) \\ &\quad + \frac{\Omega_\mu}{\xi} \sin[\xi(r,z)t_1] \delta_{26}^{i,\text{free}}(r,z,T) \\ &\quad - \frac{b_e(r,z)}{2\xi(r,z)} \sin[\xi(r,z)t_1] \Delta^{\text{free}}(r,z,T), \\ \delta_{26}^{i,(2)\mu w}(r,z,t_1) &= -\frac{\Omega_\mu}{\xi(r,z)} \sin[\xi(r,z)t_1] \delta_{26}^{r,\text{free}}(r,z,T) \\ &\quad + \frac{b_e^2(r,z) + \Omega_\mu^2 \cos[\xi(r,z)t_1]}{\xi^2(r,z)} \delta_{26}^{i,\text{free}}(r,z,T) \\ &\quad + \frac{\Omega_\mu b_e(r,z)}{2\xi^2(r,z)} \{1 - \cos[\xi(r,z)t_1]\} \Delta^{\text{free}}(r,z,T), \\ \Delta^{(2)\mu w}(r,z,t_1) &= \frac{2b_e(r,z)}{\xi(r,z)} \sin[\xi(r,z)t_1] \delta_{26}^{r,\text{free}}(r,z,T) \\ &\quad + \frac{2\Omega_\mu b_e(r,z)}{\xi^2(r,z)} \{1 - \cos[\xi(r,z)t_1]\} \delta_{26}^{i,\text{free}}(r,z,T) \\ &\quad + \frac{\Omega_\mu^2 + b_e^2(r,z) \cos[\xi(r,z)t_1]}{\xi^2(r,z)} \Delta^{\text{free}}(r,z,T). \end{aligned} \quad (56)$$

Although several numerical integrations are required in order to obtain the solution, this formal expression provides some information characterizing the low-temperature regime. Equations (50) and (52) show that the diffusion gives rise to different modes that relax at different rates so that the overall transient is not a simple exponential decay [18].

Moreover, we point out that if an atom is in a certain point of the cell at the moment of the first microwave pulse, due to the diffusion motion it will in general be in another point during the second pulse. Since b_e has a precise spatial distri-

bution, each atom experiences a Ramsey-type interrogation with unequal Rabi pulses. Their effect may not be fully averaged out in the atomic ensemble, leading to a possible shift of the observed transition.

In the high-temperature regime, the approximation (44) for population and coherence can be applied but the feedback of the cavity on the atoms is now important and the equations become nonlinear, consequently a complete numerical approach is required.

C. Detection

The free-induction decay power $P_a(t)$ dissipated in the cavity is given by the following relation [2]:

$$P_a(t) = \frac{1}{2} \hbar \omega_{26} N_a \bar{k} \frac{1}{V_a} \left| \int_{V_a} 2 \delta_{26}(r,z;t) H_{az}(r,z) dV \right|^2, \quad (57)$$

where $N_a = nV_a$ is the number of atoms in the cell of volume V_a . In Eq. (57), $t=0$ is the time at the end of the first or of the second microwave pulse and $\delta_{26}(r,z;t)$ is the free decaying coherence obtained from Eq. (49); the boundary conditions are given by the solutions previously found at the end of the first microwave pulse (48) or at the end of the second one (56).

The power coupled out of the cavity $P_d(t)$ is given by

$$P_d(t) = \frac{\beta}{\beta+1} P_a(t), \quad (58)$$

β being the cavity coupling factor. The number $N^{\mu w}$ of the detected microwave photons during the detection time t_d is

$$N^{\mu w} = \frac{1}{\hbar \omega_{26}} \int_0^{t_d} P_d(t) dt. \quad (59)$$

Relation (58) provides the atomic reference signal of the clock when operating in the passive maser mode.

In Fig. 7, we report the Ramsey patterns computed at (a) $T_0=36^\circ\text{C}$ and (b) $T_0=65^\circ\text{C}$, through Eq. (58). In the low-temperature case, we have assumed a pumping rate of $\Gamma_p=10\,000\text{ s}^{-1}$, a microwave pulse area at the center of the cell $b_{e0}t_1=1.6\pi/2$, and a laser beam diameter $\phi_L=2R=30\text{ mm}$, while in the high-temperature case we have assumed $\Gamma_p=20\,000\text{ s}^{-1}$, $b_{e0}t_1=1.45\pi/2$, and $\phi_L=2R=12\text{ mm}$.

The value assumed for $b_{e0}t_1$ corresponds to that which minimizes the Ramsey signal at $\Omega_\mu=0$; for a thin homogeneous medium, it would be $b_{e0}t_1=\pi/2$. In our case, the dependence of H_{az} on the position, the diffusion dynamics, and/or the non-null laser absorption leads to $b_{e0}t_1>\pi/2$. Moreover, this optimum value is also a function of the laser intensity; this coupling between the microwave and the laser power will be reconsidered in the next section and compared with the experimental results.

The Rabi envelopes of the Ramsey patterns of Fig. 7 are significantly determined by the total approximate decay rates of the population $\gamma_1=\gamma_{1c}+\gamma_{1se}+\gamma_d$ and of the coherence $\gamma_2=\gamma_{2c}+\gamma_{2se}+\gamma_d$; a systematic analysis shows that $\gamma_1<\gamma_2$

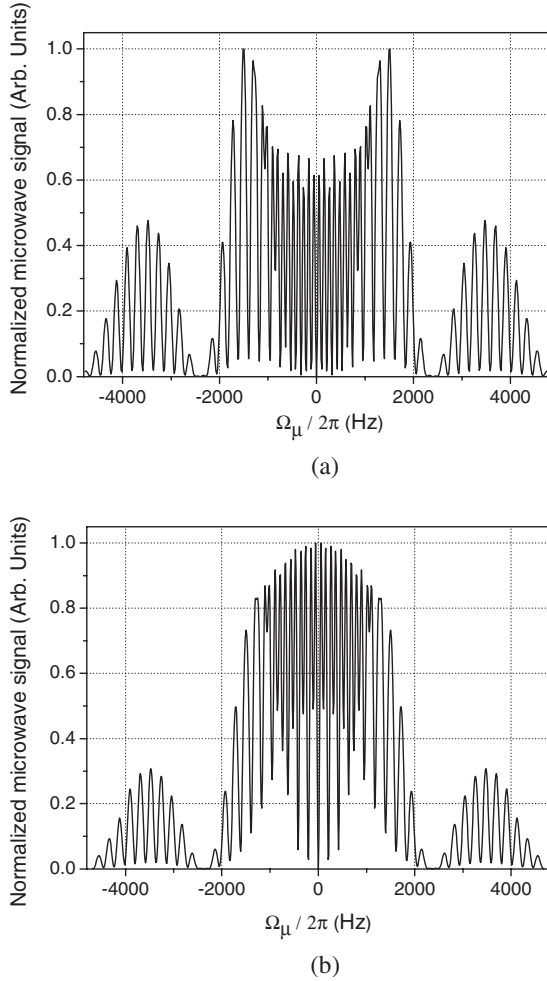


FIG. 7. Ramsey fringes computed in the microwave domain for (a) $T_0=36^\circ\text{C}$ and (b) $T_0=65^\circ\text{C}$; timing: $t_p=4$ ms, $t_1=400$ μs , $T=4.2$ ms, $t_d=2$ ms.

leads to a concavity of the envelope while for $\gamma_1 > \gamma_2$ the envelope is convex. The reduced peak-to-valley excursion of the first-neighboring fringes is due to inhomogeneities induced by the laser absorption through the cell.

When the clock is operating in the optical detection mode, the atomic reference transition is observed through the laser transmitted power after the second Rabi pulse. In this mode of operation, the laser is switched on again for a time t_d and with an intensity in principle different from that of the optical pumping phase. The laser pumping rate during the detection time will be indicated as Γ'_p . The laser power reaching the photodetector is given by

$$P_L(t) = \frac{\Gamma^* S_a}{Z_0 (d_e/\hbar)^2 S_a} \int_{S_a} \Gamma'_p(r, z=L/2; t) d\sigma, \quad (60)$$

where S_a is the laser beam section and Z_0 the vacuum characteristic impedance. $\Gamma'_p(r, z=L/2; t)$ is the laser pumping rate at the end of the cell; it is computed solving the set of Eq. (32) with boundary conditions provided by the solutions obtained at the end of the second microwave pulse (that is,

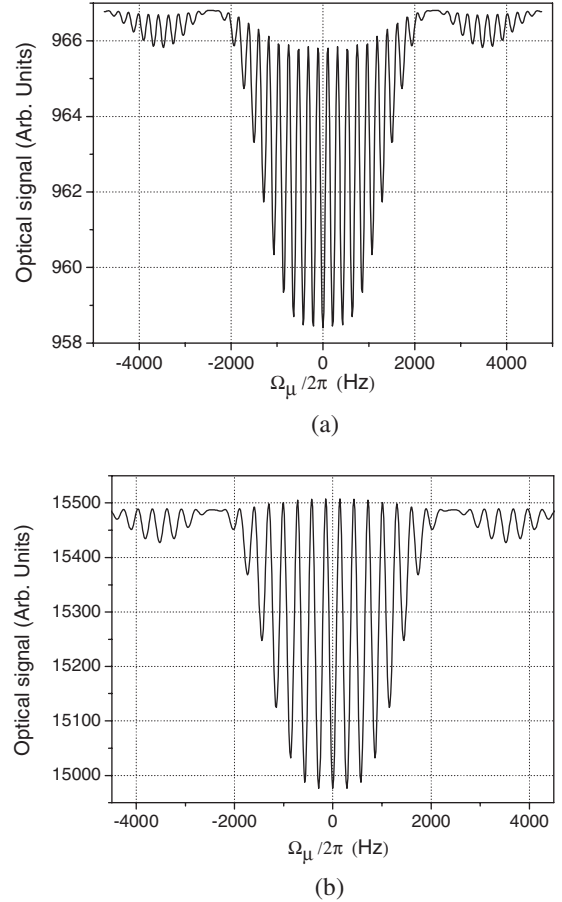


FIG. 8. Ramsey fringes computed in the optical domain: (a) $T_0=40^\circ\text{C}$, $\Gamma'_p(z=-L/2)=1000$ s^{-1} , $T=4.2$ ms; (b) $T_0=64^\circ\text{C}$, $\Gamma'_p(z=-L/2)=20\,000$ s^{-1} , $T=3$ ms.

the instant $t=0$). The number of optical photons N^{opt} reaching the photodetector is

$$N^{\text{opt}} = \frac{1}{\hbar \omega_L} \int_0^{t_d} P_L(t) dt. \quad (61)$$

In Fig. 8, we report the Ramsey pattern computed at (a) $T_0=40^\circ\text{C}$ and at (b) $T_0=65^\circ\text{C}$ through Eq. (60). In both cases, we have assumed a microwave cavity with $a=29$ mm and $d=55$ mm, a quartz cell with $R=10$ mm and $L=20$ mm, a laser beam diameter $\phi_L=15$ mm, a microwave pulse area $b_{e0}t_1=1.2\pi/2$, a pumping rate $\Gamma_p=20\,000$ s^{-1} , and a detection time $t_d=500$ μs . We have also omitted in the computations the cavity feedback terms, because in the optical detection mode a high cavity Q is not required.

The contrast C of the clock signal (peak to valley of the central Ramsey fringe) with respect to the laser background signal is shown in Fig. 9 versus the probe pumping rate Γ'_p . For high-intensity values, the probe pumps the atoms out of the clock levels, reducing the contrast as expected. The impact of the contrast value on the frequency stability will be considered in the next subsection.

D. Short-term frequency stability

The frequency stability of the passive pulsed standard in the short term is limited by the following main noise sources:

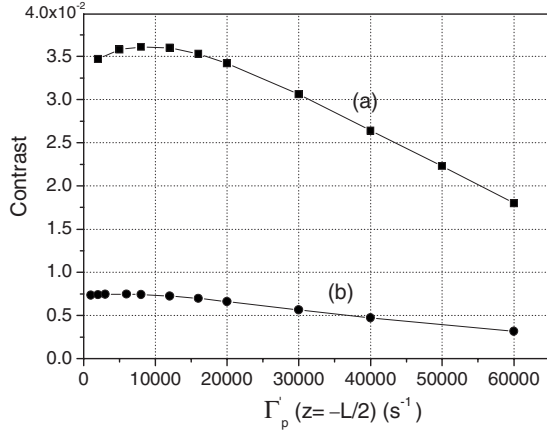


FIG. 9. Contrast of the clock signal versus the detection laser pumping rate computed for two different operating situations: (a) $T_0=64$ °C, $T=3$ ms; (b) $T_0=40$ °C, $T=4.2$ ms.

(i) thermal and shot noises of the physics package, (ii) microwave phase noise, and (iii) laser amplitude and frequency noises.

The fundamental limit to the frequency stability is due to the thermal and shot noises affecting the detected signal; in terms of Allan standard deviation $\sigma_y(\tau)$, the following well known relation holds:

$$\sigma_y(\tau) = \frac{1}{\pi Q_a R} \sqrt{\frac{T_C}{\tau}}, \quad (62)$$

where R is the signal-to-noise ratio, $Q_a=2T\omega_0/\pi$ is the atomic quality factor, and $T_C=1/f_C$ is the cycle time.

In the passive maser approach, we have [2]

$$R^{-2} = R_{\text{th}}^{-2} + R_{\text{sh}}^{-2}, \quad (63)$$

where the thermal component is given by

$$R_{\text{th}} = \sqrt{\frac{\hbar \omega_{26} N^{\mu w}}{F k_B T_0}} \quad (64)$$

and the shot-noise component is given by

$$R_{\text{sh}} = 2\pi \sqrt{\frac{N^{\mu w}}{Q_L}}. \quad (65)$$

In the above relations, F is the noise figure of the low-noise amplifier at the input of the heterodyne detector, k_B is the Boltzmann constant, T_0 is the operating cavity temperature, and $N^{\mu w}$ is the detected microwave photons number given by Eq. (59). It is important to remark that the value of R given by Eq. (63) has to be halved if a true power detector is used in the detection system [20].

In the optical detection mode, R is shot-noise-limited (counting statistics with Poisson distribution) and may be expressed as

$$R = C \sqrt{\eta_q N^{\text{opt}}}, \quad (66)$$

where C is the contrast introduced in Sec. III C, η_q is the photodetector quantum efficiency, and N^{opt} is the number of optical photons given by Eq. (61). The values of R versus Γ'_p

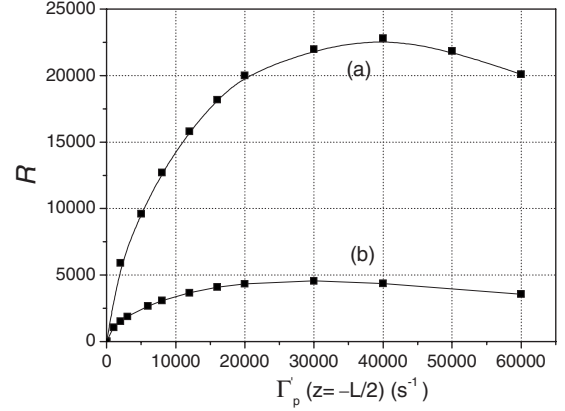


FIG. 10. Signal-to-noise ratio versus the detection laser pumping rate computed for two different operating situations: (a) $T_0=64$ °C, $T=3$ ms; (b) $T_0=40$ °C, $T=4.2$ ms.

computed for $T_0=40$ and 64 °C are plotted in Fig. 10, where we have assumed the same parameters of Fig. 8 and a photodetector quantum efficiency $\eta_q=0.8$.

In the case of passive maser mode, the frequency stability fundamental limit given by Eq. (62) can be estimated from Eqs. (57)–(59), which express the power coupled out of the cavity and the number of emitted microwave photons, and from Eqs. (63)–(65), which allow us to evaluate the signal-to-noise ratio. We first note that from Eqs. (58) and (64), the critical cavity coupling ($\beta=1$) and the minimum available noise figure F of the amplifier are required to minimize $\sigma_y(\tau)$. The other parameters influencing the frequency stability, such as the laser beam radius and intensity, cavity, and cell size, buffer gas pressure and mixture, atomic density (operating temperature), timing sequence, and so on are all linked together. Their optimization for the best stability is quite complex from the purely mathematical point of view. Therefore, as a first step, we have restricted the range of their values so that some basic requirements coming from the theoretical analysis are satisfied: (i) a strong microwave coherence extinction after the laser pulse should be assured, (ii) buffer gas pressure and composition should guarantee a good quenching of the fluorescence and at the same time produce small collision relaxation rates, (iii) the microwave field sustained by the cavity should be as uniform as possible in the active region, and (iv) a low laser absorption through the cell and a low cavity feedback are required.

Once the range of the possible values of the parameters is identified, as a second step, we have adjusted their values in order to minimize $\sigma_y(\tau)$. In this way, the physical parameters of Fig. 7(b) have been obtained, leading to

$$\sigma_y(\tau) \approx 6 \times 10^{-13} \tau^{-1/2} \quad (67)$$

for $F k_B T_0 = 5 \times 10^{-21}$ J and $\beta=1$. The above stability limit does not change considerably by varying the parameters around their optimized values, and Eq. (67) may be assumed as nearly the best achievable one for a laboratory POP maser device.

In the case of the optical detection mode, following an optimization procedure similar to that just described and as-

suming the same conditions of Figs. 8–10, the theory predicts

$$\begin{aligned}\sigma_y(\tau) &\approx 1 \times 10^{-13} \tau^{-1/2} \quad \text{at } T_0 = 40 \text{ }^\circ\text{C}, \\ \sigma_y(\tau) &\approx 3 \times 10^{-14} \tau^{-1/2} \quad \text{at } T_0 = 64 \text{ }^\circ\text{C}.\end{aligned}\quad (68)$$

A further increase of the temperature T_0 over $65 \text{ }^\circ\text{C}$ does not improve anymore the frequency stability, due to detrimental effects of the laser absorption and of the spin-exchange induced decay of the microwave coherence during the Ramsey time.

Both in the passive maser and in the optical detection operating modes, the phase noise of the microwave interrogating signal limits the achievable frequency stability (Dick effect); in the case of $\pi/2$ pulses, the limit is given by [2]

$$\sigma_y(\tau) = \left\{ \sum_{k=1}^{\infty} \text{sinc}^2\left(k\pi\frac{T}{T_C}\right) S_y^{\text{LO}}(kf_C) \right\}^{1/2} \tau^{-1/2}, \quad (69)$$

where $S_y^{\text{LO}}(f)$ is the power spectral density of the microwave fractional frequency fluctuations. The present-day state of the art of the electronics leads to $\sigma_y(\tau) \approx 1 \times 10^{-13} \tau^{-1/2}$.

In the optical detection mode, the amplitude fluctuations of the probe signal further limit the achievable stability of the POP frequency standard to

$$\sigma_y(\tau) = \frac{1}{CQ_a} \left\{ \sum_{k=1}^{\infty} \text{sinc}^2\left(k\pi\frac{T}{T_C}\right) S_{\text{AM}}(kf_C) \right\}^{1/2} \tau^{-1/2}, \quad (70)$$

where $S_{\text{AM}}(f)$ is the power spectral density of the fractional intensity fluctuations of the probe signal reaching the photodetector. It contains both the laser relative intensity noise (RIN) transferred at the output of the cell (AM-AM) and the laser frequency noise converted into amplitude fluctuations (PM-AM). We consider a distributed feedback semiconductor laser (DFB) in the constant current operation mode. Its output is amplitude squeezed [21] and its frequency spectrum is white over a broad Fourier frequency range so that the phase-diffusing field model may be assumed [22]. In this case, the PM-AM conversion gives the main contribution to $S_{\text{AM}}(f)$; even if a theoretical analysis of this conversion is quite complex for an atomic medium not optically thin [23], it is reasonable to assume $S_{\text{AM}}(f) \approx 1 \times 10^{-11} f^{-1} \text{ Hz}^{-1}$ when DFB lasers with linewidth $\Delta\nu \sim 2 \text{ MHz}$ are used. In this case, Eq. (70) leads to the limit $\sigma_y(\tau) \approx 1.1 \times 10^{-13} \tau^{-1/2}$ when $T/T_C \approx 1/2$, $f_C = 100 \text{ Hz}$, $Q_a = 6 \times 10^7$, and $C = 0.03$ ($T_0 = 64 \text{ }^\circ\text{C}$).

The results computed so far of the different noise contributions are summarized in Table I. It turns out that the fundamental stability limit of the POP frequency standard when operating in the optical detection mode is better by more than one order of magnitude with respect to the passive maser mode. Even though this limit cannot be fully achieved due to the contributions of the microwave and the laser fluctuations, the optical detection mode should allow to reach a better short-term stability with respect to the maser mode.

TABLE I. Computed frequency stability (Allan standard deviation) for an observation time of 1 s.

Sources	Passive maser	Optical detection	
	$T_0 = 64 \text{ }^\circ\text{C}$	$T_0 = 40 \text{ }^\circ\text{C}$	$T_0 = 64 \text{ }^\circ\text{C}$
Fundamental limit	6×10^{-13}	1×10^{-13}	3×10^{-14}
Microwave phase noise	1×10^{-13}	1×10^{-13}	1×10^{-13}
Laser noise		5.6×10^{-13}	1.1×10^{-13}
Final stability at $\tau = 1 \text{ s}$	6×10^{-13}	6×10^{-13}	1.5×10^{-13}

E. Residual frequency shifts

One of the main features of the POP operation is the strong rejection of the *light-shift* effect [2,4] that makes negligible its contribution to the final frequency stability of the clock; we have then omitted its analysis, assuming that the physical implementation is such that $\Gamma_{pt_p} \gg 1$ and that no laser leakage perturbs the atoms during the Ramsey interaction. The experimental results reported in the next section fully agree with this hypothesis.

Concerning the *cavity pulling* effect, the analysis reported in [4] and based on the simple three-level approach is confirmed also by the 11-level theory developed so far: a suitable microwave pulse area exists that strongly reduces the dependence of the observed clock transition on the cavity detuning.

The multilevel theory allows us to evaluate the *position-shift* effect. It is due to inhomogeneity in the physics package that makes the resonant frequencies of the Rb atoms dependent on their position inside the cell. The observed clock frequency is a weighted average of the frequencies of the single atoms, and this weighted average usually changes with laser intensity and mimics the off-resonant light-shift behavior (pseudo-light-shift). Different types of inhomogeneities may be considered; in Fig. 11 we report the computations referring to the case of Fig. 7(b) assuming a small cavity detuning. For $\psi = 0.03$ we observe at the working point $\Gamma_p = 20\,000 \text{ s}^{-1}$ a sensitivity of 1×10^{-13} for a 1% change of the laser power that may deteriorate the medium-long-term stability if the laser is not intensity-stabilized.

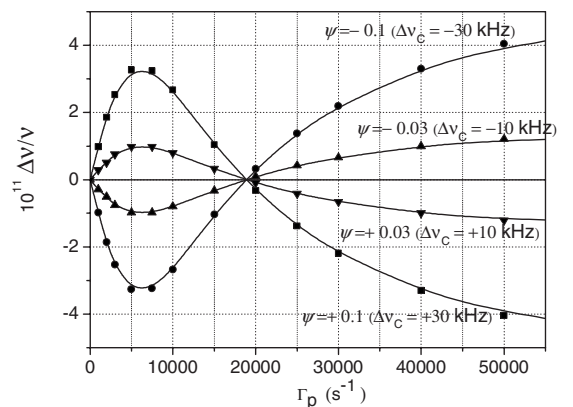


FIG. 11. Relative frequency shift of the clock transition versus the pumping rate calculated for $\psi = \pm 0.03$ and ± 0.1 .

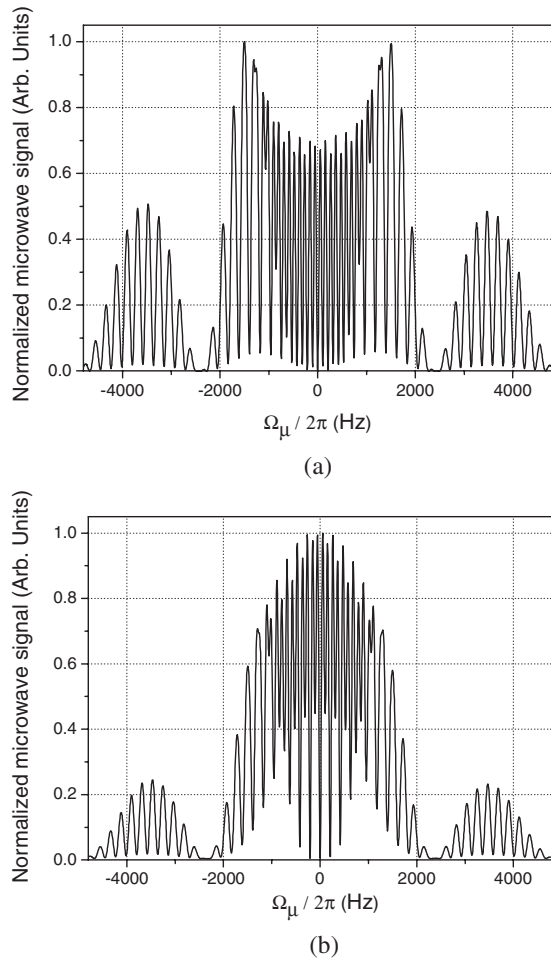


FIG. 12. Experimentally observed Ramsey fringes patterns: (a) $T_0=36$ °C ($n=3 \times 10^{10}/\text{cm}^3$, $\zeta=0.3$); (b) $T_0=65$ °C ($n=5 \times 10^{10}/\text{cm}^3$, $\zeta=5$).

Other frequency shifts affecting the long-term stability at the 10^{-14} level such as buffer gas temperature shift and gradients [24], spin-exchange shift [16], cavity temperature and mechanical stability, cavity- Q aging [25], He permeation [26], chemical Rb contaminants [27], and so on will be carefully examined in another paper.

IV. EXPERIMENTAL RESULTS

We report in this section the experimental results referring to a pulsed Rb frequency standard operating in the passive maser mode, aiming to check the theoretical predictions reported in Sec. III on the basis of the multilevel theory developed in Sec. II.

The experimental setup is similar to that described in [2], whose main physical parameters are those used in Sec. III for the numerical computations.

In Fig. 12, the Ramsey patterns are reported as observed at $T_0=36$ and 65 °C, respectively. The vertical axis is proportional to the average microwave power detected at the cavity output during the time $t_d=2$ ms. Their shapes turn out to be in very good agreement with the theoretical patterns (Fig. 7) computed for the same operating conditions.

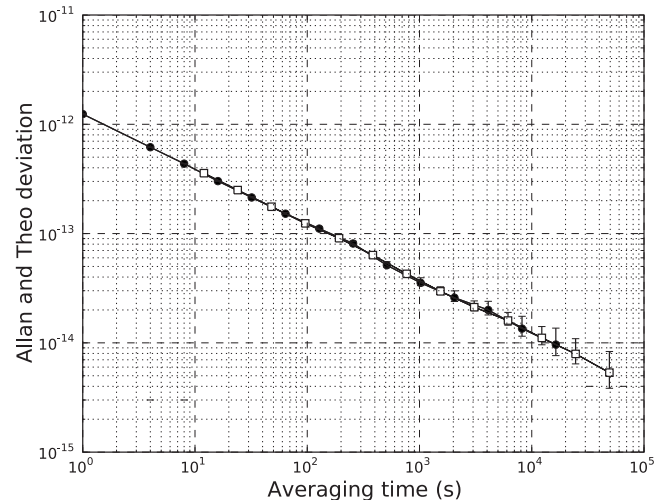


FIG. 13. Allan (black circles) and Theo (white squares) frequency standard deviations measure at $T_0=65$ °C.

The free-induction decay microwave power at $\Omega_\mu=0$ measured at the end of the first Rabi pulse is $P_d=70$ fW at $T_0=36$ °C and $P_d=20$ pW at $T_0=65$ °C, in very good agreement with the values calculated through Eq. (58), that is, 70 fW and 21 pW, respectively.

We have also performed experiments in different operating conditions, that is, (i) changing the temperature in the range $T_0=32-75$ °C, (ii) reducing the buffer gases pressure ratio in the temperature range $T_0=37-73$ °C, and (iii) changing the cell radius (from 15 to 10 mm) and the cavity length (from 37 to 55 mm). The Ramsey patterns and the detected microwave power have always been found to be in good agreement with the corresponding theoretical predictions.

In Fig. 13, we report the measured frequency stability of the POP clock at $T_0=65$ °C versus a H-maser in terms of Allan and Theo deviations, after removal of a linear drift of $8 \times 10^{-14}/\text{day}$.

We have $\sigma_y(\tau)=1.2 \times 10^{-12}\tau^{-1/2}$ for $1 \leq \tau \leq 50\,000$ s; taking into account the Dick limit due to the microwave interrogating signal [$\sigma_y(\tau) \approx 7 \times 10^{-13}\tau^{-1/2}$ [2]], we obtain $\sigma_y(\tau) \approx 1 \times 10^{-12}\tau^{-1/2}$ in perfect agreement with the theoretical prediction when $Q_a=1.2 \times 10^8$, $T_C=11$ ms, $R_{sh}=1260$, and $R_{th}=615$. The limit reported in Table I is expected for a cavity optimum coupling $\beta=1$, while in the experimental setup $\beta=0.18$. An improvement of the microwave phase noise is required to reach the stability limit predicted by Eq. (67). We have not observed any difference in the short-term stability between an ECL laser with linewidth $\Delta\nu < 0.5$ MHz and a DFB laser with $\Delta\nu \approx 20$ MHz, as expected for the passive maser mode of operation.

In Fig. 14, we report the fractional frequency shift of the POP versus the detuning $\Delta_0/2\pi$ of the laser frequency with respect to the optical absorption in the cell. The observed PM-PM conversion of $-2 \times 10^{-14}/\text{MHz}$ at $\Delta_0=0$ may well be due to a residual resonant light-shift effect: it is widely negligible in the practical applications where a frequency-stabilized laser is employed as assumed in Sec. II.

The measured dependence of the output frequency versus the laser pumping rate is shown in Fig. 15; this residual

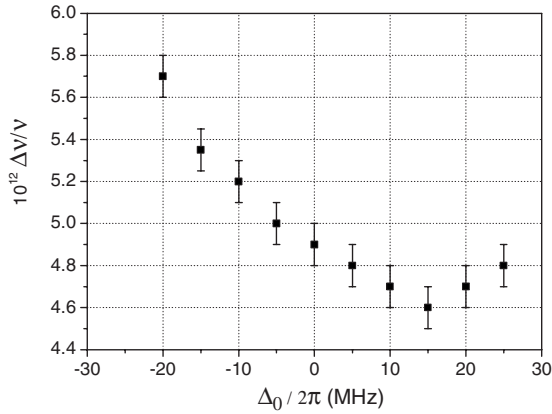


FIG. 14. Measured PM-PM conversion with $\Gamma_{p0} \approx 20\,000\text{ s}^{-1}$, $t_p = 4\text{ ms}$, $T_0 = 65\text{ }^\circ\text{C}$, $b_{e0}t_1 \approx 1.45\pi/2$, and $\psi = 0$.

AM-PM conversion may have in principle two contributions: (i) the nonresonant light-shift effect and (ii) the position-shift effect discussed in Sec. III E. The quantitative agreement between the experimental data and the theoretical prediction reported in Fig. 11 confirms that in the POP operation, the main residual source of AM-PM conversion is the position-shift effect; around the working point $\Gamma_p = 20\,000\text{ s}^{-1}$, both theory and experiment give a residual sensitivity of 1×10^{-13} for 1% of the laser intensity change. This sensitivity may be further reduced with a finer control of the cavity tuning and/or a lowered cavity feedback as it can be done in the optical detection mode where Q_L or T_0 may be lowered.

In Fig. 16, we report the observed microwave pulse area $b_{e0}t_1$ that minimizes the central Ramsey fringe at $\Omega_\mu = 0$, versus the laser pumping rate. For a thick nonhomogeneous atomic medium, its value is not only different from $\pi/2$ but depends also on the laser intensity; this coupling between the microwave and the laser powers arises through the boundary conditions among the pumping and the interrogation phases. It is well described by the developed theory as it is shown in Fig. 16, taking into account that experimental laser misalignment and mode asymmetries may increase the observed effect.

The strong damping of the Rabi oscillation is another consequence of the nonhomogeneities of the atomic medium. In

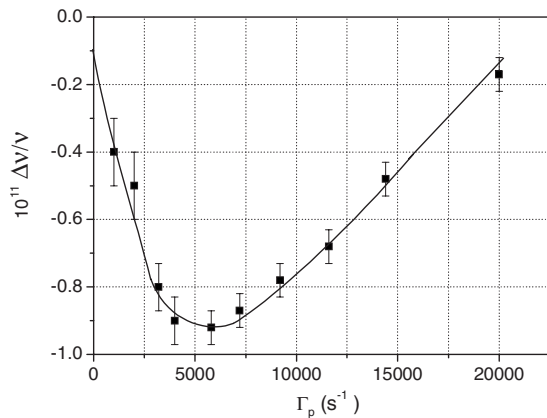


FIG. 15. Fractional output frequency versus laser pumping rate: $T_0 = 65\text{ }^\circ\text{C}$, $\psi = -0.03$ ($\Delta\nu_C \approx -10\text{ kHz}$).

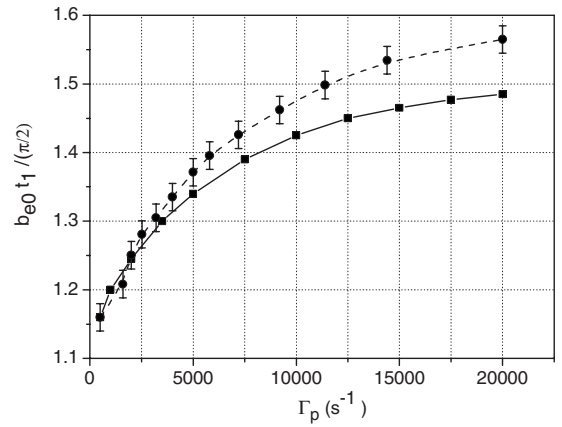


FIG. 16. Microwave pulse area for minimum Ramsey signal at $\Omega_\mu = 0$ versus Γ_p at $T_0 = 65\text{ }^\circ\text{C}$: circles: experimental data; squares: theoretical calculations.

Fig. 17, we report the measured microwave power at the end of the first Rabi pulse versus its area ($b_{e0}t_1$) with the theoretical pattern corresponding to our experimental operating conditions. A further consequence of the inhomogeneities is the spreading of the values of $b_{e0}t_1$ corresponding to the maximum Rabi envelope, minimum Ramsey fringe at $\Omega_\mu = 0$, and zero cavity pulling with respect to $\pi/2$. The good agreement between the two curves is a further check of the theory developed in Sec. II, and we can assess that the system of Eqs. (32) and their solutions discussed in Sec. III describe in a satisfactory way the behavior of the pulsed optically pumped Rb standard. Moreover, we expect that their predictions apply as well to the optical detection mode of operation, and in particular that the frequency stability limits reported in Table I will be achieved in future experiments, because both the output microwave power and the transmitted probe intensity are coupled observables of the same set of equations.

V. CONCLUSIONS

We have reported in this paper a multilevel theoretical approach for the pulsed optically pumped frequency standard

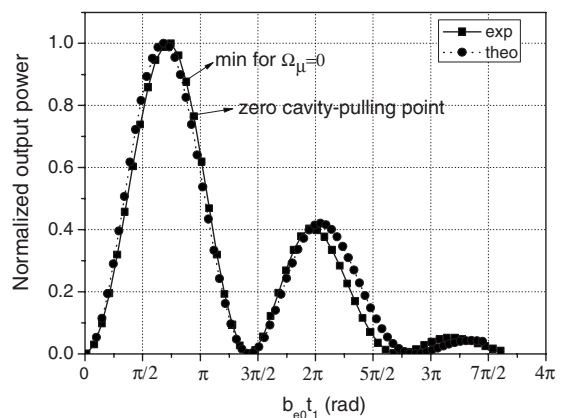


FIG. 17. Rabi oscillations: squares, experimental points; circles, theoretical calculations.

based on a vapor cell containing ^{87}Rb and buffer gas. The Rb buffer gas and spin-exchange collisions have been described with their respective Hamiltonians. In the low-temperature regime, the diffusion dynamics of the atoms into buffer gas has been considered in the numerical analysis, while in the high-density limit the laser absorption and the feedback of the cavity on the atomic ensemble have been fully taken into account.

A comparison between the theoretical predictions and the experimental results has been performed in the case of the passive maser mode of operation; a very satisfactory agreement has been found also from the quantitative point of view for the Ramsey pattern shape, the free-induction decay microwave power, the short-term frequency stability, the position shift effect, and the Rabi oscillation.

The role of the inhomogeneities in the atomic sample due to the laser absorption and to the cavity mode and detuning has been outlined, indicating the need to reduce as much as possible the nonuniformities in the physical structure in order to reduce residual AM-PM effects and unwanted couplings between laser and microwave powers.

The evaluation of the cavity-pulling and of the residual light-shift effects already provided by the three-level theory [2,4] has been confirmed by the more complete multilevel approach. We may then expect that also the theoretical predictions reported in Table I for the optical detection mode of operation will be achieved in future experiments leading to

frequency stabilities not far from that reached by active H masers.

It is important to remark anyway that the shot noise-limit is not the whole of the story as far as the final frequency stability of the standard is concerned. In fact, the microwave phase noise and the probe signal AM and FM fluctuations may overcome significantly the theoretical physical limit in the short term, independently of the physical approach adopted such as buffer gas or coated cells, POP, or pulsed EIT.

In the medium-long term, the POP frequency stability is expected to be better with respect to other schemes [28,29] due to its very low residual conversions of the pumping laser fluctuations into the output frequency (Figs. 14 and 15).

Finally, we observe that the theory reported here foresees a better short-term frequency stability for the optical detection mode, provided stable enough (AM and FM) lasers may be used or a stability similar to that reached in the passive maser mode but at a lower operating temperature, which may be of great benefit from the power dissipation point of view and for the medium-term stability of the standard.

ACKNOWLEDGMENTS

This work has been partially supported by the Italian Space Agency (ASI Contract No. I/057/06/0).

-
- [1] A. Godone, F. Levi, S. Micalizio, E. K. Bertacco, and C. Calosso, *IEEE Trans. Instrum. Meas.* **56**, 378 (2007); S. Guerandel, T. Zanon, N. Castagna, F. Dashes, E. de Clercq, N. Dimarcq, and A. Clairon, *ibid.* **56**, 383 (2007).
- [2] A. Godone, S. Micalizio, F. Levi, and C. Calosso, *Phys. Rev. A* **74**, 043401 (2006).
- [3] C. O. Alley, in *Quantum Electronics*, edited by C. H. Townes Editor (Columbia University Press, New York, 1960); M. Arditi and T. R. Carver, *IEEE Trans. Instrum. Meas.* **13**, 146 (1964).
- [4] A. Godone, S. Micalizio, and F. Levi, *Phys. Rev. A* **70**, 023409 (2004).
- [5] J. Vanier and C. Audoin, *The Quantum Physics of Atomic Frequency Standards* (Adam-Hilger, Bristol, England, 1989).
- [6] T. C. English, E. Jechart, and T. M. Kwon, in *Proceedings of the 10th Precise Time and Time Interval Forum, Washington, 1978*, edited by L. J. Rieger (NASA, Maryland, 1979), pp. 147–165.
- [7] Actually there is also the relaxation rate of the excited state Γ^* that is related to a homogeneous broadening of the optical line due to buffer gas collisions; however, usually it is verified that $\Gamma^* \gg \gamma_1, \gamma_2$ and the adiabatic approximation allows us to express the optical coherences and excited-state populations in terms of the ground-state observables.
- [8] A. Godone, S. Micalizio, and F. Levi, *Metrologia* **45**, 313 (2008).
- [9] A. R. Edmonds, *Angular Momentum in Quantum Mechanics* (Princeton University Press, Princeton, NJ, 1974).
- [10] J. C. Camparo, *J. Chem. Phys.* **126**, 244310 (2007); P. J. Oreto, Y.-Y. Jau, A. B. Post, N. N. Kuzma, and W. Happer, *Phys. Rev. A* **69**, 042716 (2004).
- [11] M. A. Bouchiat, J. Brossel, and L. C. Pottier, *J. Chem. Phys.* **56**, 3703 (1972).
- [12] F. A. Franz, *Phys. Rev.* **141**, 105 (1966).
- [13] F. Gong, Y. Y. Jau, and W. Happer, *Phys. Rev. Lett.* **100**, 233002 (2008).
- [14] J. Vanier, C. Jacques, and C. Audoin, *Phys. Rev. A* **31**, 3967 (1985).
- [15] M. O. Scully and M. Suhail Zubairy, *Quantum Optics* (Cambridge University Press, Cambridge, UK, 1997).
- [16] S. Micalizio, A. Godone, F. Levi, and J. Vanier, *Phys. Rev. A* **73**, 033414 (2006).
- [17] W. Demtroder, *Laser Spectroscopy: Basic Concepts and Instrumentation*, 3rd ed. (Springer, Berlin, 2003).
- [18] M. E. Wagshul and T. E. Chupp, *Phys. Rev. A* **49**, 3854 (1994); D. Suter, *ibid.* **46**, 344 (1992).
- [19] W. Franzen, *Phys. Rev.* **115**, 850 (1959); J. A. Valles and J. M. Alvarez, *Phys. Rev. A* **50**, 2490 (1994); P. Minguzzi, F. Strumia, and P. Violino, *Nuovo Cimento B* **46**, 145 (1966).
- [20] C. Calosso, S. Micalizio, A. Godone, E. k. Bertacco, and F. Levi, *IEEE Trans. Ultrason. Ferroelectr. Freq. Control* **54**, 1731 (2007).
- [21] T. Yabuzaki, T. Mitsui, and U. Tanaka, *Phys. Rev. Lett.* **67**, 2453 (1991).
- [22] R. Walser and P. Zoller, *Phys. Rev. A* **49**, 5067 (1994).
- [23] J. C. Camparo, *J. Opt. Soc. Am. B* **15**, 1177 (1998); J. C.

- Camparo and J. G. Coffey, Phys. Rev. A **59**, 728 (1999); J. G. Coffey, M. Anderson, and J. C. Camparo, *ibid.* **65**, 033807 (2002); M. Huang, J. G. Coffey, and J. C. Camparo, Opt. Commun. **265**, 187 (2006).
- [24] M. Huang, J. G. Coffey, and J. C. Camparo, Phys. Rev. A **75**, 052717 (2007).
- [25] J. G. Coffey, B. Sickmiller, and J. C. Camparo, IEEE Trans. Ultrason. Ferroelectr. Freq. Control **51**, 139 (2004).
- [26] J. C. Camparo, C. M. Klimcak, and S. J. Herbulock, IEEE Trans. Instrum. Meas. **54**, 1873 (2005).
- [27] B. Patton, K. Ishikawa, Y.-Y. Jau, and W. Happer, Phys. Rev. Lett. **99**, 027601 (2007).
- [28] R. Boudot, S. Guerandel, E. de Clercq, N. Dimarcq, and A. Clairon, IEEE Trans. Instrum. Meas. (to be published).
- [29] G. Mileti, Jinqun Deng, F. L. Walls, D. A. Jennings, and R. E. Drullinger, IEEE J. Quantum Electron. **34**, 233 (1998).